Hydrogeological study of the Glencoe Corobrik Factory Site, KwaZulu-Natal Province, South Africa

Maserole Elvis Moabelo
Student Number: 562585

A Research Report submitted to the Faculty of Science, University of the Witwatersrand, Johannesburg, in partial fulfilment of the requirements for the degree of Master of Science in Hydrogeology

Supervisor: Prof. Tamiru Abiye
School of Geosciences
University of the Witwatersrand, Johannesburg

December 2020

DECLARATION

I declare the **Hydrogeological study of the Glencoe Corobrik Factory Site, KwaZulu-Natal Province, South Africa** is my own work and has been submitted for the Master of Science in Hydrogeology at the Faculty of Science, University of the Witwatersrand, Johannesburg ONLY. All the sources used and quoted in this paper have been referenced and acknowledged.

M.E Moabelo

Signed: Maserole Elvis Moabelo

Date: 17 December 2020

ABSTRACT

Hydrogeological conditions at the Glencoe Corobrik Factory, KwaZulu-Natal, South Africa, are investigated in this study. The general geology of the area is made up of the Ecca Group metasedimentary sequence of the Karoo Supergroup. A hydrogeological conceptual site model is developed based on the data acquired during the study. The methods of data collection involved borehole drilling and logging, aquifer tests, water sampling and analyses. Aquifer tests were conducted using a slug test method on two newly drilled boreholes for this research. The calculated hydraulic conductivity and transmissivity values are 0.014 m/day and 0.033 m/day, 0.44 m^2/day and 1.19 m^2/day for BH01 and BH02, respectively. The underlying rocks are sandstones and siltstones of the Vryhied Formation that constitute the main lithology for the aquifer in the area. Dolerite dykes may be interfingered with the sandstones at depth, creating a flow barrier and conduit in some places. The weathered aquifer is made up of the upper sequence sandstones, while the dolerite emplacement presents a secondary fractured aquifer. Groundwater chemistry is dominated by two water types; Ca^{2+}- HCO_3^- and Na^+- HCO_3^-. The Durov diagram points to ion exchange processes where Ca^{2+} is exchanged for Na^+. The groundwater chemistry is influenced by weathering processes (silicates). The study revealed human activities have a low influence on the groundwater chemistry in the area. The Ca^{2+} and Mg^{2+} vs SO_4^{2-} plots provided crucial evidence that the groundwater has not been influenced by acid mine drainage even though the area was previously dominated by coal mining activity. Surface water chemistry is represented by Ca^{2+}- HCO_3^- water type with Mg^{2+}- SO_4^{2-} and Na^+- HCO_3^- also occurring as minor water types. Most samples are clustered towards the region of Mg^{2+}- SO_4^{2-}, indicating a possible influence of sulphates that may be derived from the old mine dumps on the surface. Based on the current hydrochemical data, groundwater and surface water have distinct geochemical compositions, which implies that contaminants emanated from surface processes have less influence on the deep groundwater system. Results from the stable isotopes also support the hydrochemical results suggesting a very minimal link between the groundwater and surface water based on the current sampling. Groundwater samples were recharged directly from rainfall prior to evaporation, while surface water samples show an evaporation effect. Surface water samples showed an evaporation effect with an evaporation equation of $\delta D = 4.31\ \delta^{18}O+7‰$ with a R^2 value of 0.98.

ACKNOWLEDGEMENTS

This research report was made possible by the Council of Geoscience, Corobrik Glencoe and Itasca Africa. I am thankful to Prof. T Abiye, my supervisor who reviewed this work and made sure it was to a standard that is acceptable in the science fraternity. I am grateful to the staff at Itasca Africa for their review of the report. A special vote of thanks to Mrs. C Kraak who did the fieldwork with me. Ms. D Duthe is also thanked for this opportunity.

I would also like to thank my family for their continued support. To my parents (Mr and Mrs Moabelo) who always pushed me and made sure I reach the finish line, thank you!

Ke ya bo koko Maserole, koko Chuene le rakgolo Sebushi, ke a leboga.

Ke leboga Modimo wa Thaba ya Sione.

WITS UNIVERSITY

TABLE OF CONTENTS

LIST OF FIGURES

LIST OF TABLES

LIST OF APPENDICES

LIST OF ABBREVIATIONS

K	hydraulic conductivity
m	metres
m/day	metres per day
AMD	acid mine drainage
m^3	cubic metres
m^3/ day	cubic metres per day
mamsl	metres above mean sea level
mbs	metres below surface
mbgl	metres below ground level
$kg.m^{-3}$	kilogram per cubic metre
l/s	litres per second
mm	millimetre
°C	degrees Celsius
WMA	Water Management Area
EOH	end of hole
mg/L	milligram per litre
SANS	South African national standards
SAWS	South African Weather Services
VSMOW	Vienna Standard Mean Ocean Water
GMWL	Global Meteoric Water Line
LMWL	Local Meteoric Water Line

1.0 INTRODUCTION

The Glencoe Corobrik Factory is situated near the town of Glencoe in the KwaZulu-Natal Province, South Africa. The town was dominated historically by coal mining, which has left a significant footprint, both on the surface and underground (Corobrik Pty Ltd, 2017). Part of the property is a servitude (coal discard dumps) that belongs to the Department of Mineral Resources. The factory produces bricks using the Ecca Group shales as the raw material. Two active quarries are currently being mined in the study area. The Glencoe Corobrik Factory wishes to apply for a Water Use License to the South African Department of Water and Sanitation. One of the requirements for the application is a hydrogeological study of the area. This independent research report focuses on the hydrogeological investigations of the site.

The study area is conceptualised by the development of a conceptual hydrogeologic model in order to understand the hydrogeology of the site. The model will identify or characterise the hydrochemistry of the groundwater, identify any geologic structures as part of the conceptual hydrogeologic model. Stable isotope analysis will also be used to identify any interconnection between groundwater and surface water.

1.1 BACKGROUND

Groundwater in South Africa is generally of better quality, and safer for domestic use compared to surface water. This is because surface water is more readily exposed to pollutants. Groundwater is thus a valuable water resource in South Africa (Lapworth *et al*., 2017).

Many human activities impact negatively on the groundwater resources, particularly mining (Prathap and Chakraborty, 2019). Chemicals (organic and inorganic) can infiltrate into the groundwater and are the primary source for groundwater pollution (Mohanty *et al*., 2018). The general approach in groundwater monitoring is first to obtain a sample, which represents a baseline water condition; this will inform if there is a contamination or not, if so, what type of contamination is there? It then becomes essential to continue monitoring the water quality to ensure that contaminants do not spread further. At the time of this investigation, only surface water was monitored quarterly in the study area with no groundwater monitoring. As it was already stated, it is a requirement that a groundwater study to be commissioned for a Water Use License to be granted, hence the purpose of the original study.

In South Africa, coal is used for the generation of electricity by ESKOM (South African electricity public utility). It is also used in the production of liquid fuels by the South African Synthetic Oil Limited (SASOL) (Hancox and Gotz, 2014). It is the largest source of non-renewable fuel for electricity generation in South Africa with 96 % of electricity generated from coal-fired power stations (Hancox and Gotz, 2014). Coal mining, therefore, plays a vital role in South Africa's economy through power generation and exports of the raw material to other countries (Barnes and Vermeulen, 2012).

Coal mining and the processing therein result in large quantities of waste rock and tailings being generated and exposed. This is the primary cause of contamination that impacts the environment in mining areas (Cravotta, 2005). The deterioration of groundwater quality due to the generation of acidic water (acid mine drainage), which subsequently mixes with the surrounding water resources, is a challenge in coal mining areas (Mohanty *et al*., 2018). Groundwater contamination and the related consequences from coal mining and related activities have been reported by several authors (Cravotta, 2005; Lei *et al*., 2009; McCarthy, 2013; Campaner *et al*., 2014; and Lghoul *et al*., 2014).

Mining, especially for gold and coal, has the most severe impact on water resources, as often the processes form Acid Mine Drainage (AMD). AMD is caused when sulphide is exposed to water and oxygen (mediated by bacteria). The occurrence of AMD is natural, the process is only accelerated by mining activities due to the exposure of sulphide bearing rocks (Akhil and Koldas, 2006). The elevated concentrations of sulphate, acidity, and metals in abandoned mines resulting from flooding of underground mines or seepage from waste dumps often impair the use of water due to the degraded water quality caused by the exposure of metals to water and oxygen (Cravotta, 2005). Sulphides react with water and oxygen forming sulphates, with bacteria often acting as a catalyst to the process. The higher acidity increases the solubility of metals, which causes contamination and toxicity to groundwater resources. This toxicity makes groundwater unfit for human consumption and operational processes in most industries (McCarthy and Humphries, 2013).

The Northfield Colliery operated to the west of the current mining site from 1981 to the early 1990s. The mine produced about 55 000 tonnes of coal per month from underground workings (Hancox and Gotz, 2014). There is a pile of old discarded dump and workings from coal mining in the property that is not owned by Corobrik Glencoe. These old coal mining activities are likely

to have impacted the water quality due to runoff and infiltration of precipitation in the form of rainfall and may have likely influenced the chemistry of the groundwater on site.

1.2 PROBLEM STATEMENT

Coal mining in Glencoe and around the factory site has ceased, leaving behind mined-out voids, quarries, and waste discard dumps. Corobrik (Pty) Ltd, the Glencoe Factory site, is partially underlain by old underground mine voids and part of the property is a servitude occupied by a coal discard dump. As part of the factory Water Use License application, a hydrogeological study is required. The hydrogeological study includes hydrogeological characterisation of the aquifer and the hydrochemistry of the groundwater on the factory site. Thus, hydrogeological and hydrochemical characterisation of the groundwater around the Glencoe Corobrik Factory is important in order to understand the groundwater dynamics of the area. This will include the identification of ions that influence the geochemical composition of groundwater, identifying hydrochemical facies and the origin of groundwater. The end product of this study will be a hydrogeological conceptual model.

1.3 AIM AND OBJECTIVES

This study aims to define the hydrogeology of the site and to characterise the chemistry of the water bodies and identifying any hydrogeological processes that contribute to the chemistry of the water. A conceptual model is employed in the current study to conceptualise the hydrogeological dynamics of the site. The conceptual hydrogeological model was intended to assist in the understanding of groundwater conditions and hydraulic connections. To achieve the project aim, the following objectives were set:

- Characterise groundwater hydrochemistry,
- Define interaction between surface water and groundwater, and
- Establish a baseline water quality within the site.

2.0 LITERATURE REVIEW

2.1 HYDROCHEMISTRY

Groundwater and surface water quality is variable spatially and controlled primarily by the host rock chemistry and by many factors such as anthropogenic activities within a region. The pollution of groundwater is a challenge for many regions around the world (Tarawneh *et al*., 2019). It is then of paramount importance to quantify groundwater quality that is utilised for commercial, industrial, municipal, and domestic water supply. This helps in the sustainable development and proper groundwater resource management. Physical, chemical, and bacterial characteristics of water are used to describe the quality of groundwater (Al-Aboodi *et al*., 2008). A conceptual hydrogeological model requires information from groundwater chemistry, as it can inform us whether there are any sources for contamination within a particular study area, as well as source-path receptors.

Measurements of major constituents indicate possible processes and reactions that may be occurring in a particular aquifer. It also provides a means to identify the dissolved mineral species present in the aquifer, leading to an understanding of the history of water-rock interaction in the aquifer (Wilson, 2005).

Lithological units have distinct mineral compositions, the chemistry of groundwater is, therefore, dependent on the type of the host lithology. It is, therefore, accepted that different water types will be realised in different lithological settings. In the current study, a Piper diagram is used to identify water types and subsequently identifying the water quality.

2.2 ENVIRONMENTAL ISOTOPES

Most groundwater studies are concerned with the residence time of water or the source of the water, including its flow paths (Mook, 2000). This can be achieved through the use of tracers. Stables isotopes can be applied in hydrogeological studies as tracers. They can inform us about distinct sources and sinks within a hydrological system (Mook, 2000). The isotope results obtained from hydrological studies are often useful when interpreted along with other data such as groundwater chemistry (Hamdi *et al*., 2018).

Groundwater studies focussing on the origin of groundwater, compared to their residence times, apply stable isotopes and radiogenic isotopes, respectively. This is because stable isotopes are

conservative and will not easily interact with other mineral species within the system. Oxygen-18 and deuterium are the most commonly used stable isotopes as they form part of the water molecule, which makes them ideal tracers for this application (Mazor, 2004).

The analysis of stable isotopes is reported and expressed in comparison to a known standard sample. The Vienna Standard Mean Ocean Water (VSMOW) is the most commonly used standard. The isotopic composition of water is expressed in per mil (‰) deviations from the VSMOW standard (Mazor, 2004).

Mazor (2004) noted that water entering a hydrological system carries the distinct fingerprint of its origin, making it possible to trace where the water in the system comes from. Kendall and Caldwell (1999) also noted that rainwaters have a different isotopic signature from water that already exists within a catchment. These distinctive signatures would result in different water samples plotting on different positions on the δD and $\delta^{18}O$ plot with respect to a meteoric water line. Fractionation processes such as evaporation and condensation will cause the deviation of water from the meteoric water line. This would be indicative of the respective processes taking place prior to recharge (Mazor, 2004). The stable isotopes of ^{18}O and D are used in this study to trace the interaction between groundwater and surface water, and the possible source of the groundwater is inferred.

2.3 CONCEPTUAL HYDROGEOLOGICAL MODELLING

Conceptual hydrogeological modelling has proved to be a useful tool for groundwater practitioners, for groundwater planning and management. Singhal and Gupta (2010) described different uses for groundwater modelling as follows:

- Modelling the effect of groundwater stress by using predictive models,
- Management of groundwater to ensure the sustainability of aquifers, and
- Estimation of contaminant transport and the injection thereof.

A model is a representation of a real system or a process. As in many other disciplines, three main components make up a complete groundwater study. These are data, conceptualisation, and numerical modelling (Figure 2-1). A conceptual model hypothesises how the real system would work (Konikow and Reilly, 1999), as it considers hydrogeological data, i.e. water level

measurements, geological logs, hydraulic properties, and hydrogeochemical data, to conceptualise the existing situation of a system. However, it is extremely difficult, or impossible, to represent all the dynamics of the system being studied (Singhal and Gupta, 2010).

The development of a conceptual hydrogeological model is a prerequisite to conduct a numerical model. The resulting conceptual model is a simplified visual representation of the complex groundwater system within the study area. Aquifer layers, with aquifer properties, layer types, and boundary conditions are amongst other components that make up a conceptual model. Similar hydrostratigraphic units with the same hydrogeological parameters are defined. These units are then classified according to their properties as either aquifers or aquitards. Aquifer properties, which are essential in characterising the hydrostratigraphic units and govern groundwater flow include porosity, hydraulic conductivity, and specific yield. It is vital to accurately predict the direction and rate of groundwater flow and contaminant transport. This is critical for groundwater remediation planning and implementation (Bear *et al*., 1992). There are three recognised different types of models in the literature, depending on the purposes (Wilson, 2005):

- Interpretive models – used for organising data or studying the system dynamics,
- Predictive models – used to predict how the system may react in the future due to future reactions or conditions, and
- Generic models – in this model type, hypothetical hydrogeological systems are studied and analysed.

An interpretive model was used in the current study. This type of model is the best option for organising and merging different data that can be interpreted together to understand the system dynamics. A conceptual model represents field conditions more accurately the more input data it has. Therefore, it is vital that the model be dynamic and continuously updated as data become available. The resulting conceptual model should be as simple as possible but also represent the system behaviours accurately (Yang *et al*., 2010). The approaches and methodologies described so far are used to compile a conceptual model for the study area based on the available data. Consequently, a reasonable assumption can be deduced where needed.

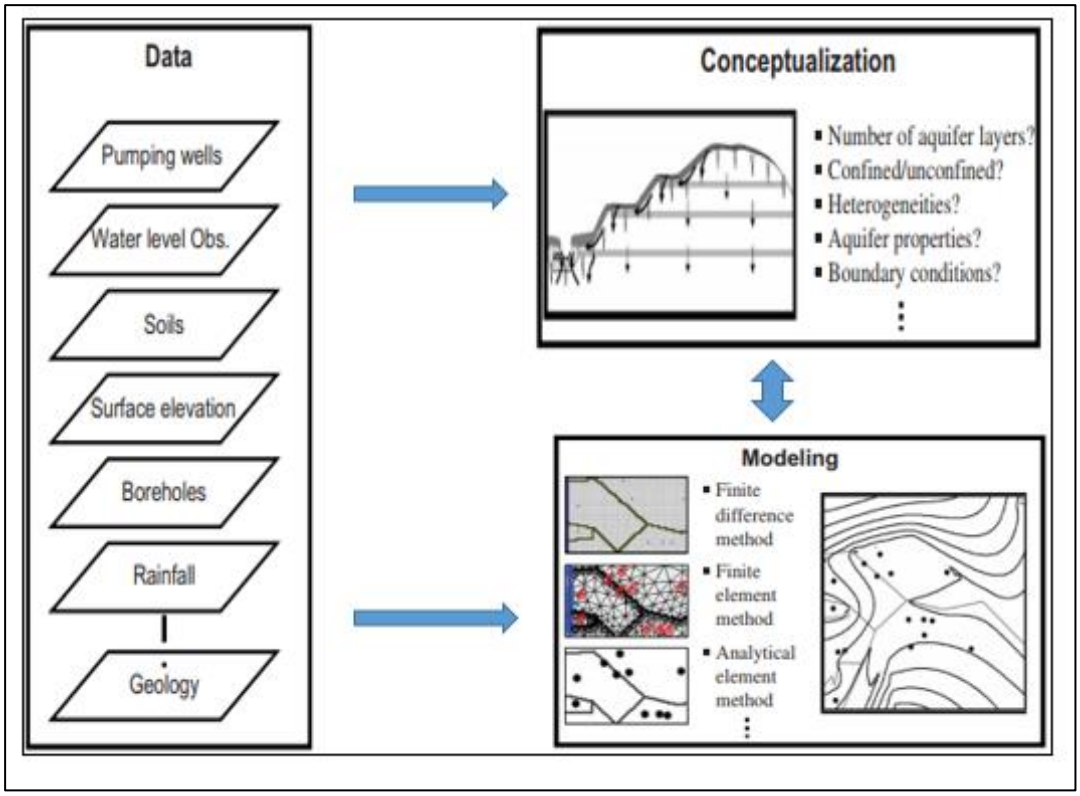

Figure 2-1: Three components of groundwater studies (Source: Maidment and Hopper, 2005 in Yang et al., 2010).

3.0 DESCRIPTION OF THE STUDY AREA

3.1 LOCATION

The Corobrik (Pty) Ltd Glencoe Factory is situated 3.6 km to the northwest of Glencoe town, which is 10 km west of Dundee in the KwaZulu-Natal Province, South Africa, (Figure 3-1). The factory is located within the Klip River Coalfield in the Vryhied Formation. The study area straddles two quaternary catchments, namely V32E and V60D in the Thukela Water Management Area (WMA). The Thukela WMA is estimated to cover over 29 046 km^2, of which 783 km^2 and 308 km^2 is covered by quaternary catchments V32E and V60D, respectively.

The study area falls within the Endumeni Local Municipality, which belongs to the uMzinyathi District Municipality. The main towns within the local municipality are Glencoe, Dundee, and Wasbank. The Endumeni local municipality has a total population of 64 862 people, with 83.2 % of the population living in the urban area (Statistics South Africa, 2011).

The area is also characterised by old underground mine workings, which are identifiable by the mine dumps on the surface. Underground mine voids also occur in the study area and are assumed to be approximately 10 km wide, however, the depth is unknown (Corobrik Pty Ltd, 2017).

Figure 3-2 shows the layout of the site, including the areas that are believed to be old underground coal mine workings (Corobrik Pty Ltd, 2017).

Figure 3-1: Locality map showing the study area in red square which is 3.6 km NW of Glencoe. The inset map shows a zoomed clip of the study area with quaternary catchment V60D and V32E shown.

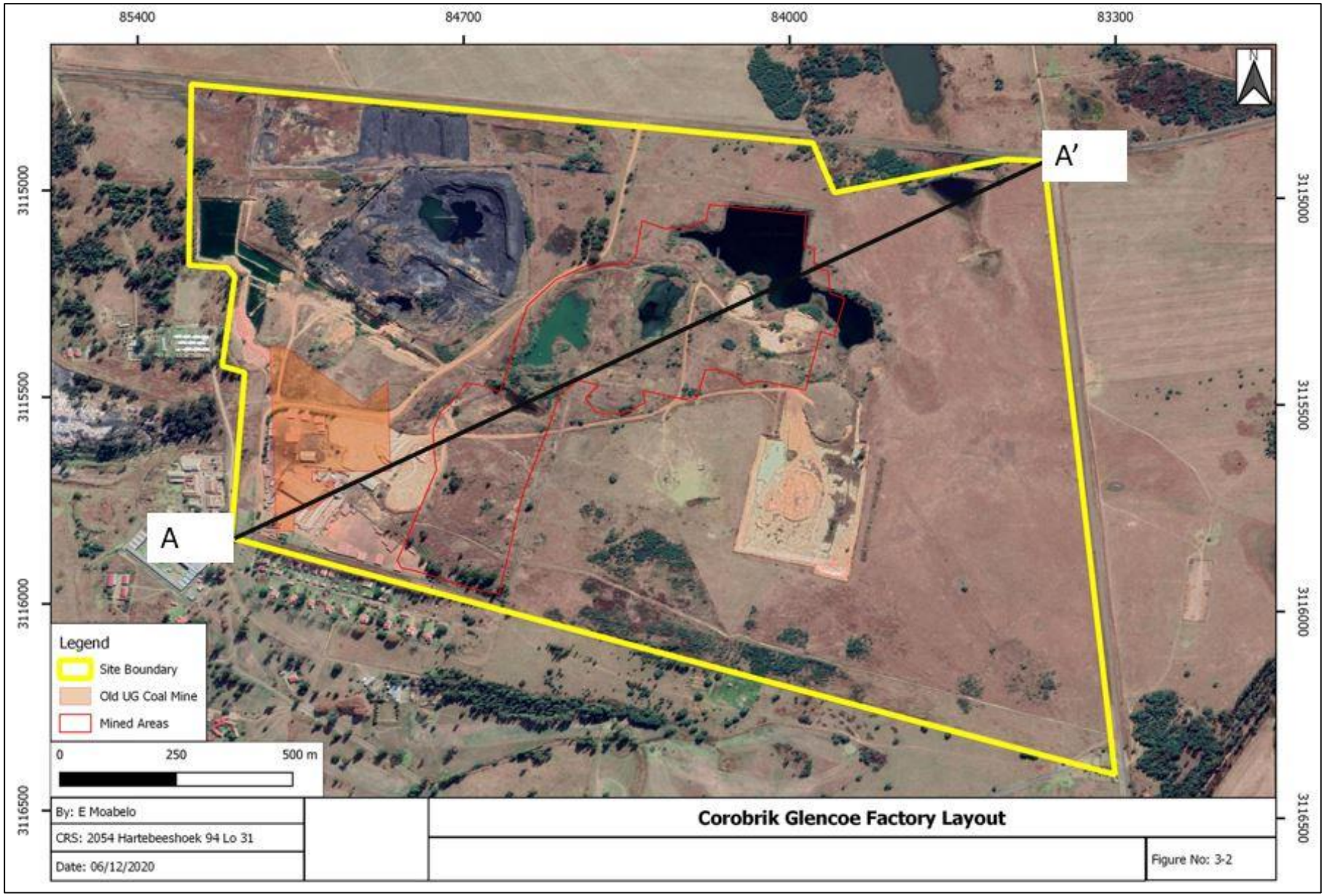

Figure 3-2: Factory layout for the Corobrik Glencoe site. Coal mined out areas are delineated.

3.2 SITE DESCRIPTION

Raw materials for bricks such as shale and siltstone are mined during the dry winter months. Mining is conducted for three to five months depending on raw material requirements from quarries up to a maximum depth of 15 m on average to the sandstone floor (Corobrik Pty Ltd, 2017).

There are several quarries found in the property, five of which have been mined-out, and have subsequently filled up with rainwater (Figure 3-2). The resulting volumes as per the register are listed in Table 3-1. The active quarries are the Silt Quarry, located on the eastern portion of the property, and the Lottering Quarry on the western side, which produces the non-silty material (Figure 3-2). The Lottering Quarry does not exceed 8 m in-depth, and the Silt Quarry does not exceed 15 m depth. The section of the Silt Quarry that is currently being mined is at a maximum depth of 10 m. From June 2016 to July 2017, municipal water consumption ranged from 1200 to > 2000 m^3/month or around 24 000 m^3/year (Corobrik Pty Ltd, 2011).

Table 3-1. Corobrik Glencoe quarry water volumes (Source: Corobrik Pty Ltd, 2011).

Quarry Details	Latitude	Longitude	Volume (m^3)
Quarry 1	-28.14771	30.14435	151 336
Quarry 2	-28.14912	30.14203	58 382
Quarry 3	-28.14961	30.13995	57 569
Quarry 4	-28.14902	30.13439	36 271
Quarry 5	-28.14744	30.13235	39 096

3.3 CLIMATE, TOPOGRAPHY AND VEGETATION

Monthly rainfall and temperature data were obtained from the South African Weather Services (SAWS), station number 03708563 – Newcastle for the dates ranging from 1995 to 2017. The rainfall data is presented in Figure 3-3 with temperature data presented in Figure 3-4.

The rainfall season occurs between November and March, while the dry months extend from April to September. The month of October is intermediate between dry and wet. The dry months are also accompanied by cold conditions with temperatures reaching lows of 14 °C in July. Average temperatures for Glencoe range from 14 °C in winter months to 21 °C in summer months.

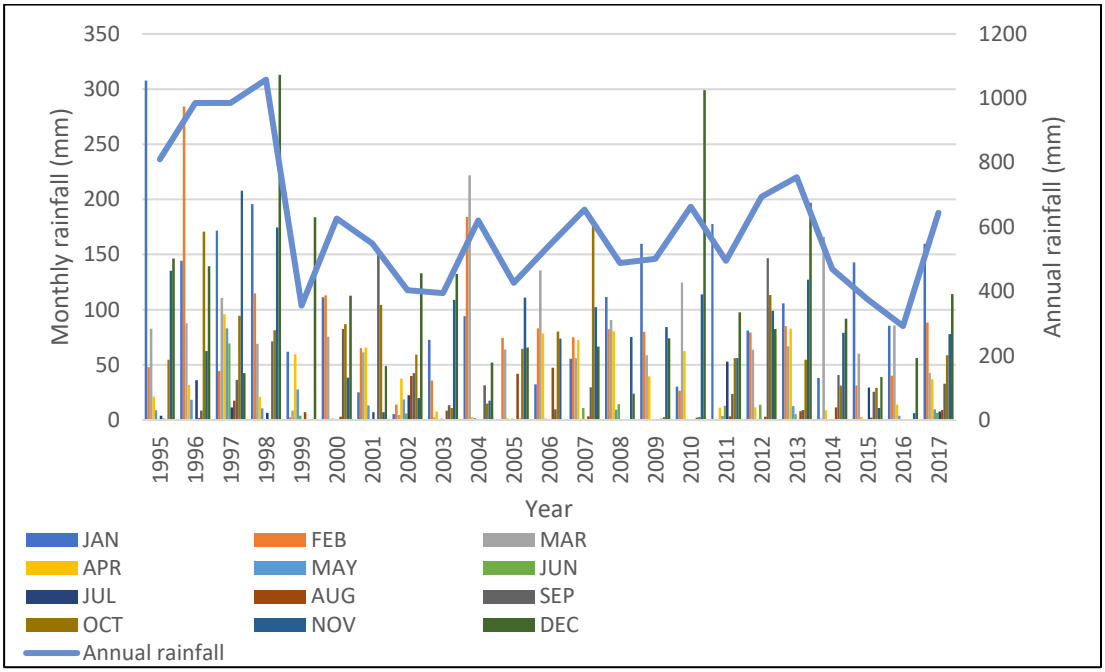

Figure 3-3: Plot showing the monthly rainfall and the annual rainfall for the study area (Data source: SAWS, 2017).

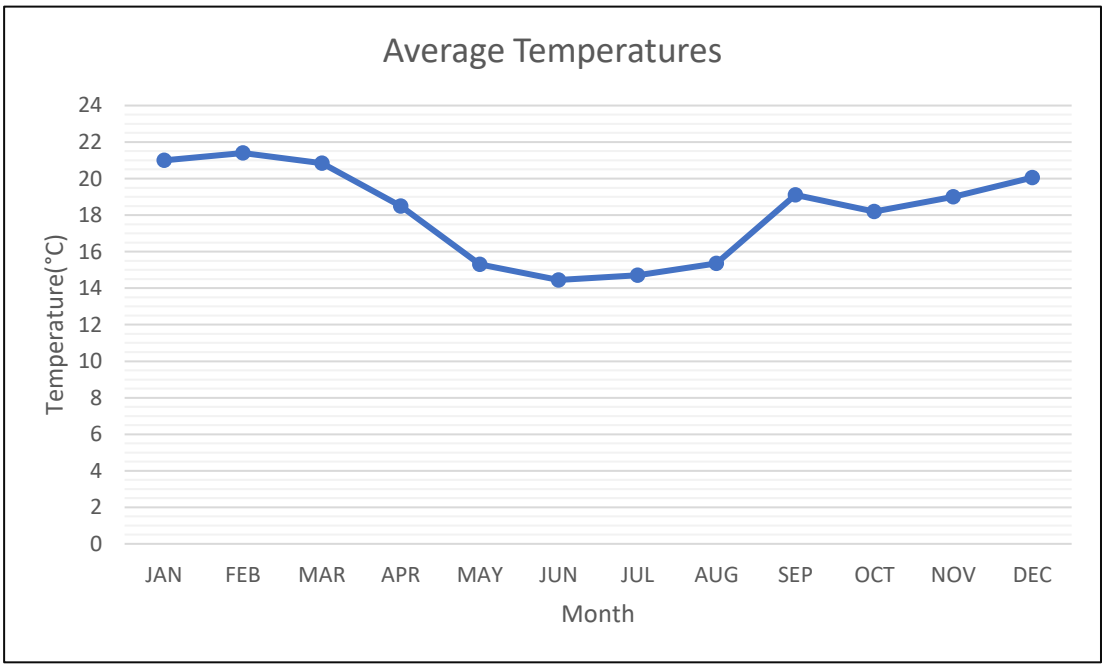

Figure 3-4: Plot showing average monthly temperatures for the study area (Data source: SAWS, 2017).

The area around the study area is generally flat with elevations ranging from 1370 mamsl to 1345 mamsl, the average slope is estimated to be less than 3 %. Looking at all the cardinal directions, no mountains exist in the immediate vicinity of the site confirming its flatness and a gentle slope.

The area surrounding the study site is mostly used for commercial farming, with most farmers growing crops and cattle farming is also common.

3.4 GEOLOGY

3.4.1 Regional Geology

The area is underlain by the late Carboniferous (310 Ma) to Mid Jurassic (185 Ma) sedimentary rocks of the Karoo Supergroup (Woodford and Chevallier, 2002). The Karoo Basin covers an area of approximately 700 000 km^2 and has a total thickness of approximately 12 km in the main basin (Catuneanu *et al*., 2005). The geology of the area is shown in Figure 3-5, with the study area represented with a red border.

The Karoo Basin is a retro-arc foreland basin. It has a south-westerly dip and is bound by the Cape Fold Belt on the south and underlain by the Kaapvaal Craton in the north and the Namaqua-Natal metamorphic belt in the east (Uys, 2007). The Karoo Supergroup hosts five Groups, from youngest to oldest; the Dwyka Group, Ecca Group, Beaufort Group, Stormberg Group, where the sequence is covered by the basaltic flood lavas of the Drakensberg Group (Catuneanu *et al*., 2005).

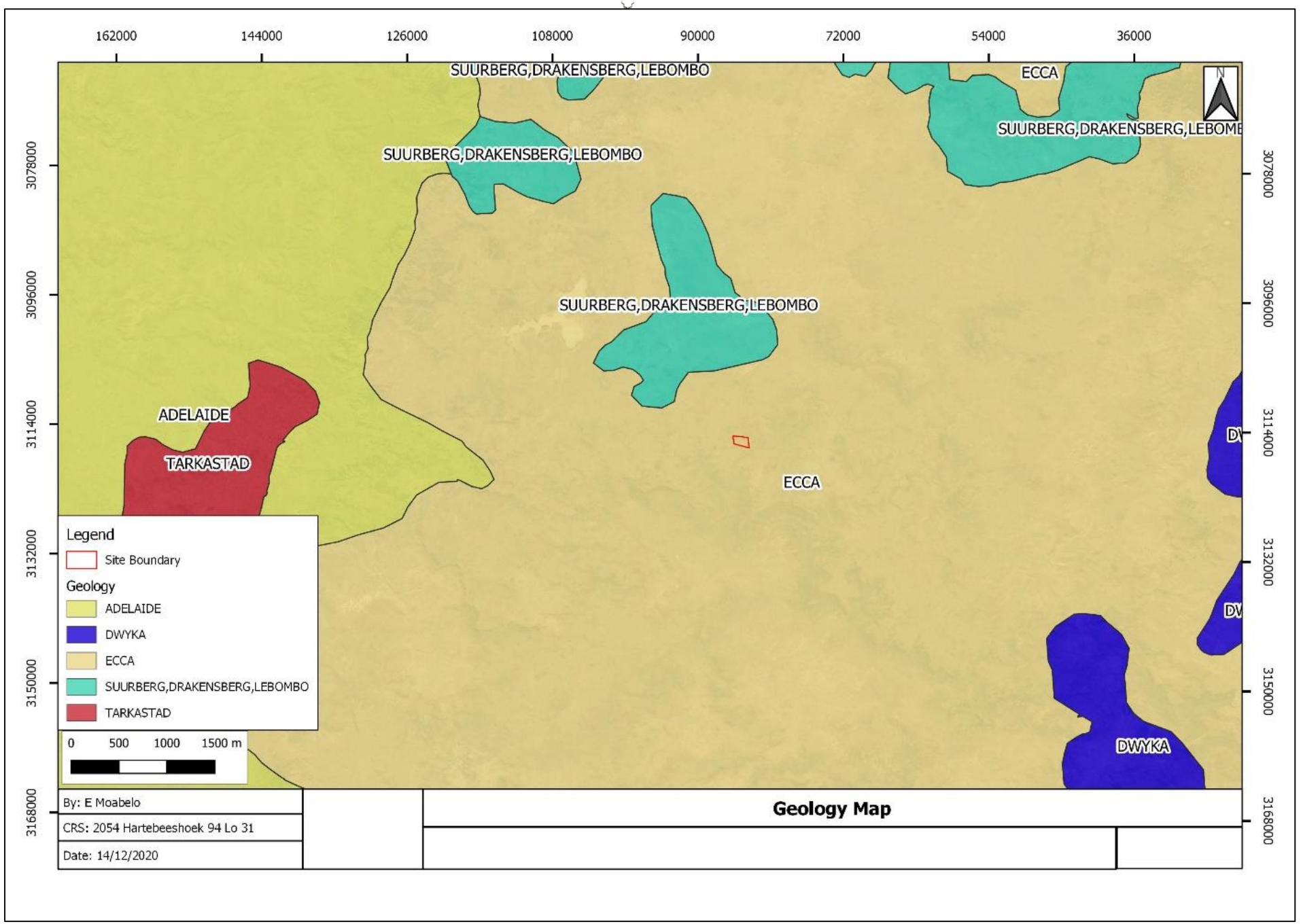

Figure 3-5: Geology of the area, the study area is shown with a red border line.

3.4.2 Local Geology

The local geology is composed of the Ecca Group rocks of the Karoo Supergroup (Johnson *el al*, 2006). According to Johnson *et al*. (2006), the early to late Permian Ecca Group has a total of 16 Formations, which consist primarily of shallow marine and deltaic facies sediments. This succession is characterised by lateral facies changes and is categorised as follows:

- South, west and northwest facies – Prince Albert and Whitehill Formations,
- Southern facies – Collingham, Vischuil, Laingsburg, Ripon, Fort Brown, and Waterford Formations,
- Western and the north-western facies – Tieberg, Skoorsteenberg, Kookfontein and Waterford Formations,
- North-eastern facies – Pietermaritzburg, Vryheid, and Volksrust Formations.

The study area hosts the north-eastern facies, the Vryheid Formation, which comprises of shale, mudstone with a coarsening in the upward sequence. This Formation overlies the Dwyka Group, making it the lowermost Formation of the Karoo Supergroup in the north-eastern part of the Karoo Basin (Johnson *et al*., 2006).

The Vryheid Formation comprises of feldspathic sandstone, shale, mudstone, and coal seams. The study area falls specifically in the Klip River coalfield, which exploits the coal seams of the Vryheid Formation. The coal seams were previously peat swamps that developed on alluvial plains and the back swamps (Hancox and Gotz, 2014). The economically exploitable coal seams occur in the fluvial succession (Hancox and Gotz, 2014). The Vryheid Formation in this area has a total thickness of approximately 310 m, where regionally the total thickness of this Formation extends to approximately 500 m (Hancox and Gotz, 2014). The variation in thickness is caused by the uneven topography of the pre-Karoo surface. The Vryheid Formation has a generally upward-coarsening lithofacies arrangement (Johnson *et al*., 2006). As indicated in the regional geology, the area is underlain by Ecca Group sediments of the Karoo Supergroup. A cross-section through the study area is presented in Section 6.0.

3.4.3 Field Observations

The local geology is comprised mainly of metasedimentary sequence of the Vryhied Formation. Weathered shales from this Formation can be seen in the field (Figure 3-6), which contains a ferricrete layer. The ferricrete has nodules that can allow water to sit in; this type of process can form perched aquifers (Figure 3-7). The ferricrete is red, which is influenced by the presence of oxides. From the stratigraphic section in Figure 3-6, the sandstones are not visible anywhere in the property. Geological logging of the drill chips reveals that sandstones do exist in the area. From the logs, it is observed that these sandstones occur below the shale units.

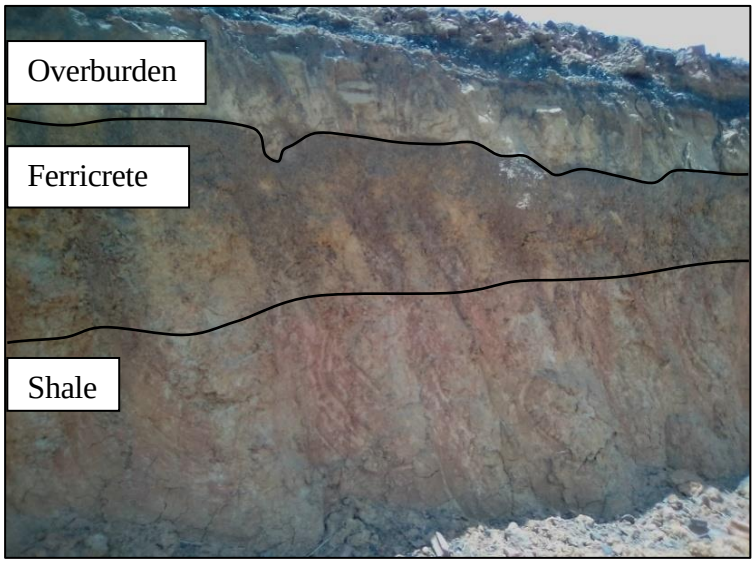

Figure 3-6: Stratigraphic Section in Quarry 5 with visible overburden soils underlain by ferricrete layer with shales at the bottom of the succession

Figure 3-7: In-Situ observation of a ferricrete with nodules.

3.4.4 Geological Structures

Faulting that is caused by the intrusion of dolerite dykes and sills and extensional tectonics is common in the area, causing visible, and large displacements. These events were associated with the break-up of Gondwana. Hancox and Gotz (2014) also observed displacements within the Klip River coalfield, the maximum recorded displacement is 137 m, with 229 m uplift that is measured up north of the Klip River coalfield. Four major dolerite sills have been described in the region, from youngest to oldest: the Zuinguin, Utrecht, Lugogo and Talana dolerites (Hancox and Gotz, 2014).

3.5 HYDROGEOLOGY

3.5.1 General Hydrogeology

The area is underlain by intergranular and fractured aquifers, with secondary porosity being the main media for groundwater flow. Groundwater occurs along faults, joints and the Karoo dolerite contacts within the regional hard rocks (Henning, 2016). According to the aquifer classification scheme by Matoti *et al*. (1999), the area hosts a minor aquifer, which is defined as fractured rocks with low primary permeability. These aquifers can also include other rock units of different permeability with varying water quality.

According to the Department of Water Affairs and Forestry (2004) the sandstones make up the best aquifers in the Thukela WMA. Groundwater yield is approximately 0.1 l/s to 0.6 l/s. Groundwater recharge estimate reported in the literature for the Thukela WMA is in the range of 15 – 20 mm/yr (Umgeni, 2019).

3.5.2 Groundwater levels

Based on the fieldwork results, two groundwater levels are found to exist in the property. The ferricrete layer, which resulted in the perched aquifer at approximately 4 - 8 mbgl. The regional groundwater level rests between 15 - 19 mbgl with the average groundwater level at 12 mbgl. Figure 3-8 shows groundwater levels measured during the fieldwork on the available boreholes. Although no time-series data were available for groundwater levels, these data give enough information about the current groundwater levels on site.

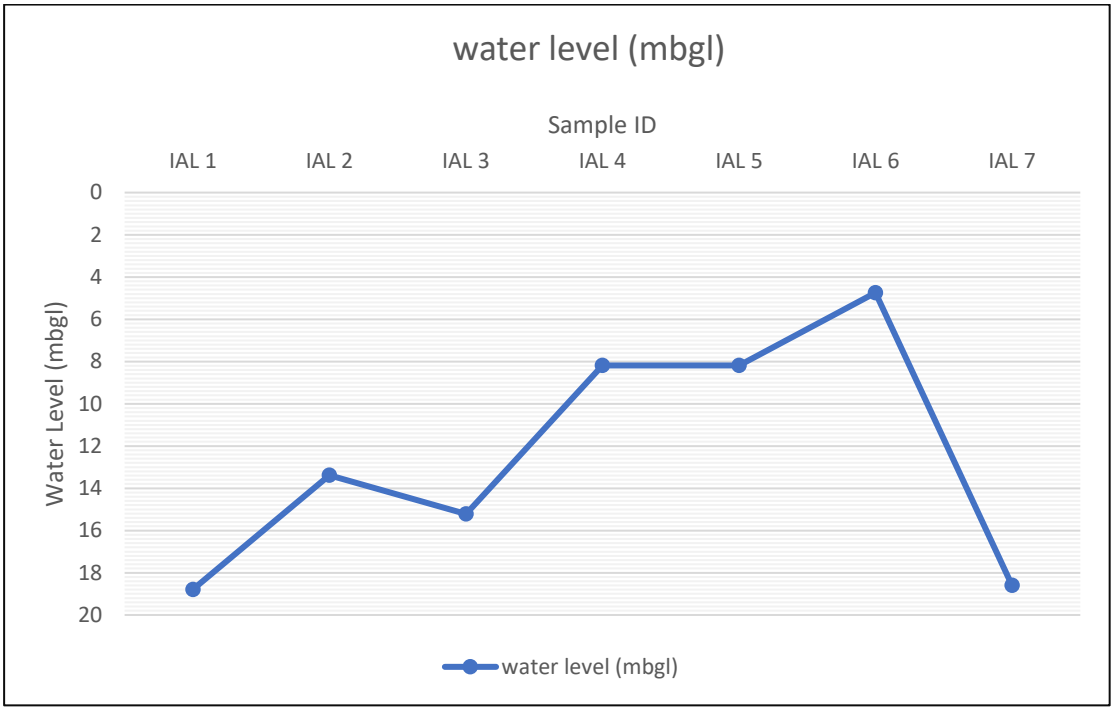

Figure 3-8: Groundwater levels measured on-site in September 2018.

4.0 METHODOLOGY

4.1 DESKTOP STUDY

The methodology used in this study included the review of existing literature for the site since this is an existing operational factory. Many studies have been conducted before including hydrochemical analysis. The literature on the geology and hydrogeology of the region was also reviewed as part of the desktop study. Data from SAWS were also reviewed as part of the desktop study and were analysed to give an understanding of the climate in the study area.

4.2 FIELDWORK

Different tasks were carried out in order to collect different data and merge them to compile a conceptual model. A combined approach, including the use of chemical and isotope analysis, was used. Aquifer properties were also estimated from two drilled boreholes for this study. Chemical, stable isotope and aquifer property data were collected during the six-day field trip that was undertaken from the 11th to the 16th of September 2018 at the Glencoe Corobrik site. Other supporting field activities that were conducted on-site included drilling supervision and the logging of the drill chips.

To fulfil the aim and objectives of this study, various fieldwork procedures outlined in this subsection were followed.

4.2.1 Site selection

The project area straddles two quaternary catchments, so the drilling locations of the three new boreholes had to be strategic so that the two catchments could be represented. A layout map of the area with 5 m contours overlaid on satellite imagery, was used to assist in predicting general groundwater flow directions and identifying suitable drilling locations.

Water samples were collected at several locations on-site, which included the quarry sites and new boreholes, for water chemistry and isotopic analysis. Another three water samples for offsite water bodies were also collected for inclusion into the water quality dataset, which also included groundwater and surface water bodies.

4.2.2 Drilling programme

In order to understand the subsurface dynamics, borehole drilling was undertaken using a percussion rig (Figure 4-1). In total, three boreholes were sited and drilled within the study area. This comprised of two 50 m deep boreholes and one 150 m deep borehole. All three boreholes were designed to be completed with two shallow and deep Polyvinyl Chloride (PVC) pressure pipes installed. The shallow and deeper aquifers were to be studied using the two PVC pressure pipes installed, respectively. It is also important to mention that another purpose for the deeper borehole (150 m) was to intersect the old underground mine workings.

Figure 4-1: Drilling in progress for borehole 1 (BH01).

Each borehole was chip logged during drilling, from the chips, the lithological logs (Figure 4-2) were constructed using Strater Software. The full lithological logs are presented in Appendix 1, including the final borehole construction details. The summary of these borehole details are shown in Table 4-1. Spreadsheets of the borehole logs are appended to this report as Appendix 2.

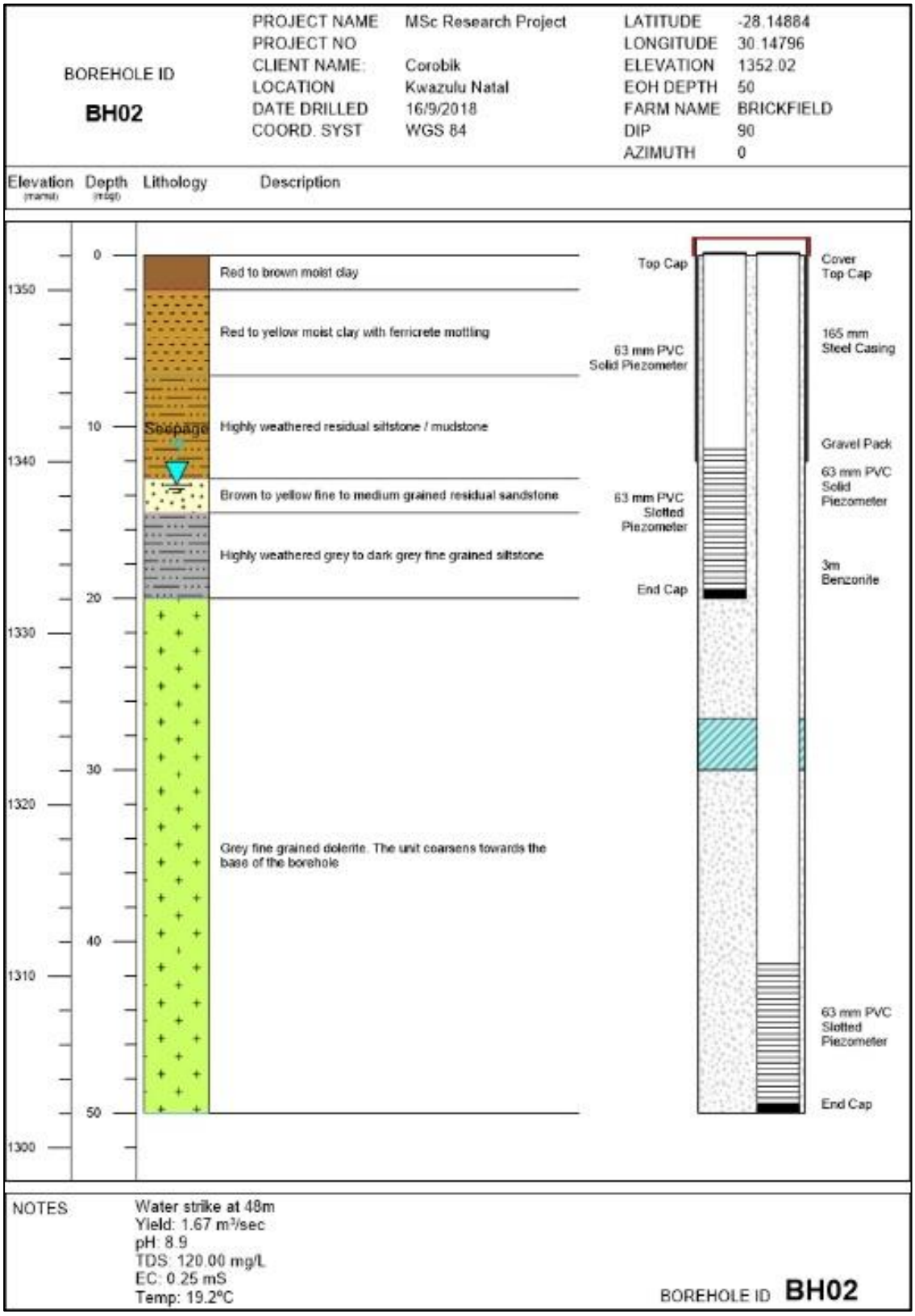

Figure 4-2: Borehole log constructed for drilling site BH02, including well construction scheme.

Table 4-1: The Corobrik Glencoe Borehole details.

Borehole Number	BH01	BH02 Deep	BH02 Shallow	BH03 Shallow	BH03 Deep
Latitude	-28.1461	-28.1488	-28.1488	-28.1402	-28.1402
Longitude	30.1332	30.1480	30.1480	30.14895	30.1490
BH Depth (m)	50	50	20	20	50
Annulus Diameter (mm)	165	165		165	
Steel Casing Depth (m)	12	12		12	
Bentonite Thickness (m)	15-20	17-20		17-20	
Fill	Gravel	Gravel		Gravel	
Casing Diameter (mm)	63	63		63	
Solid PVC Screens (m)	41.3	41.3	21.3	21.3	41.3
Slotted PVC screens (m)	8.7	8.7	8.7	8.7	8.7
Water Level (mbgl)	18.79	13.38	15.22	Dry	24

4.2.3 Sampling procedure

During the six days spent on-site, 23 water samples were collected for analysis. Appendix 3 shows a list of collected samples, while Figure 4-3 shows the location of the sample position. These included eight samples for chemical analysis (anions, cations, and metal analysis), and 15 samples for isotopic analysis. The sampling protocol and procedures followed are described below.

For the identification of samples, labels were prepared and were filled in on-site and stuck on the bottles. Corresponding information was noted in the field notebook for reference purposes. The information documented included the sample name, *in-situ* physiochemical parameters (pH, EC, TDS, and temperature), date, time of sampling and the GPS coordinates (Appendix 3).

High-density polyethylene (HDPE) plastic bottles were used for both types of samples collected. One litre (1 L) bottles were used for collecting samples to be analysed for the chemical analyte. Fifty millilitres (50 ml) bottles were used for collecting samples for isotopic analysis, these sampling bottles had double caps. On both occasions, the sample bottles were rinsed at least five times before the collection of the actual sample that was sent to the laboratory for analysis.

Isotope samples were collected according to a standard procedure as described by Mook (2000). The D-excess is calculated using the Local Meteoric Water Line (LMWL), the formula is expressed as:

Equation 1

$d = \delta D - 5.7 * \delta^{18}O$

The local meteoric line is referenced from studies done in the region (e.g. Weitz and Demlie, 2013 and Mduduma, 2018) and is referred to as the LMWL in this study.

The dams were sampled directly with the sample bottles by submerging the bottles below the water level in the dams. For boreholes, a bailer was used to collect samples. The boreholes were purged five times before collecting the actual sample using a bailer. The bottles were filled to the top with water, avoiding any entrainment of air bubbles.

Sampling for chemical analysis, a standard procedure as outlined by the Department of Water Affairs and Forestry (2006) was followed. The samples were not acidified and no titration test was performed on-site for the total alkalinity. To compensate for the former, the bottles were kept in a cooler box with ice for the duration of the field campaign and were later refrigerated and kept cool at 4 °C while waiting to be transported to the laboratory for analysis.

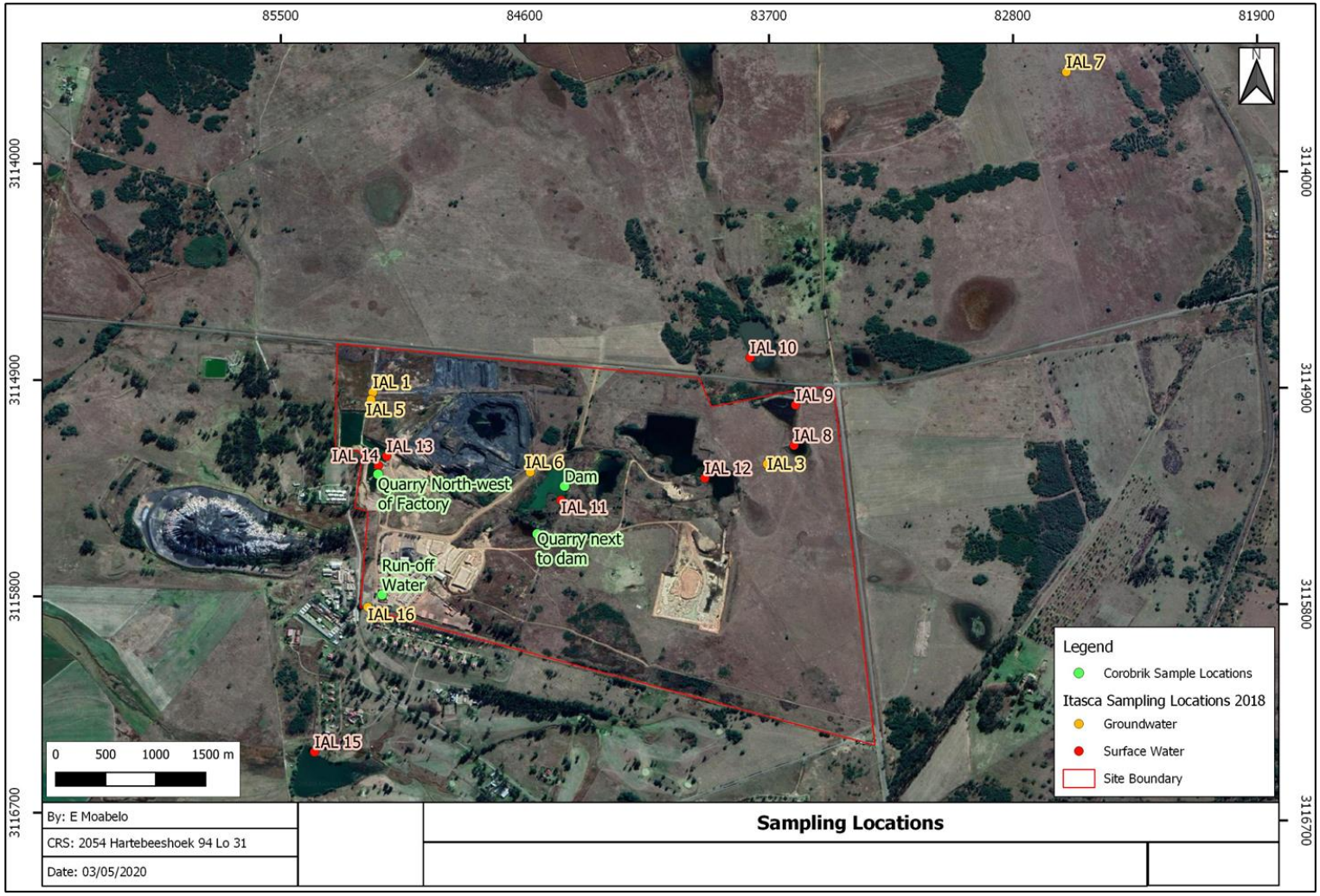

Figure 4-3: location map showing sampling points on the factory property and off the property of Corobrik Glencoe.

4.3 HYDROCHEMICAL ANALYSIS

Water quality analyses for metals, major cations and anions were conducted at the M and L laboratories in Johannesburg.

Physiochemical parameters were measured in the field, which included temperature, pH, EC, and TDS. These field measurements were taken using the Hanna instrument with the pH/EC/TDS and temperature probe. All field measured parameters are presented in Appendix 3. The instrument was calibrated before the field campaign based on the instructions as outlined in the user manual.

Stable isotope analyses were conducted at the iThemba Environmental Isotope Laboratory in Johannesburg. The equipment consists of a Los Gatos Research Liquid Water Isotope Analyser. The precision for Oxygen and Hydrogen are estimated to be 0.5 ‰ and 1.5 ‰, respectively.

4.4 TEST PUMPING

Slug testing was conducted to measure the hydraulic conductivity of the aquifer. A slug of the known volume was lowered into a well to displace (rise or fall) the water level, the rate at which the water level responds to the change is then measured against time. A dipmeter was used to measure the water level response, and a stopwatch was used to measure the time (Figure 4-4).

Figure 4-4: Slug testing borehole 1 (BH01) on the study location.

In the current study, AQTESOLV software was used for interpreting the data using the Bouwer-Rice method. This method can be used in both confined and unconfined aquifers. The method works on two assumptions: the elastic storage mechanisms' effects are neglected, and the water table level remains constant. The method works with both isotropic and anisotropic conditions (Ismael, 2016). The following equation is used to calculate hydraulic conductivity. Figure 4-5 shows the Bouwer-Rice slug test method configuration.

Equation 2

$$\ln\left(\frac{H(t)}{H_o}\right) = -\frac{2K_r bt}{r_c^2 \ln\left(\frac{R_e}{r_{w*}}\right)}$$

Where: $r_{w*} = r_w(K_z/K_r)^{1/2}$, each parameter is explained in Section 5.1.

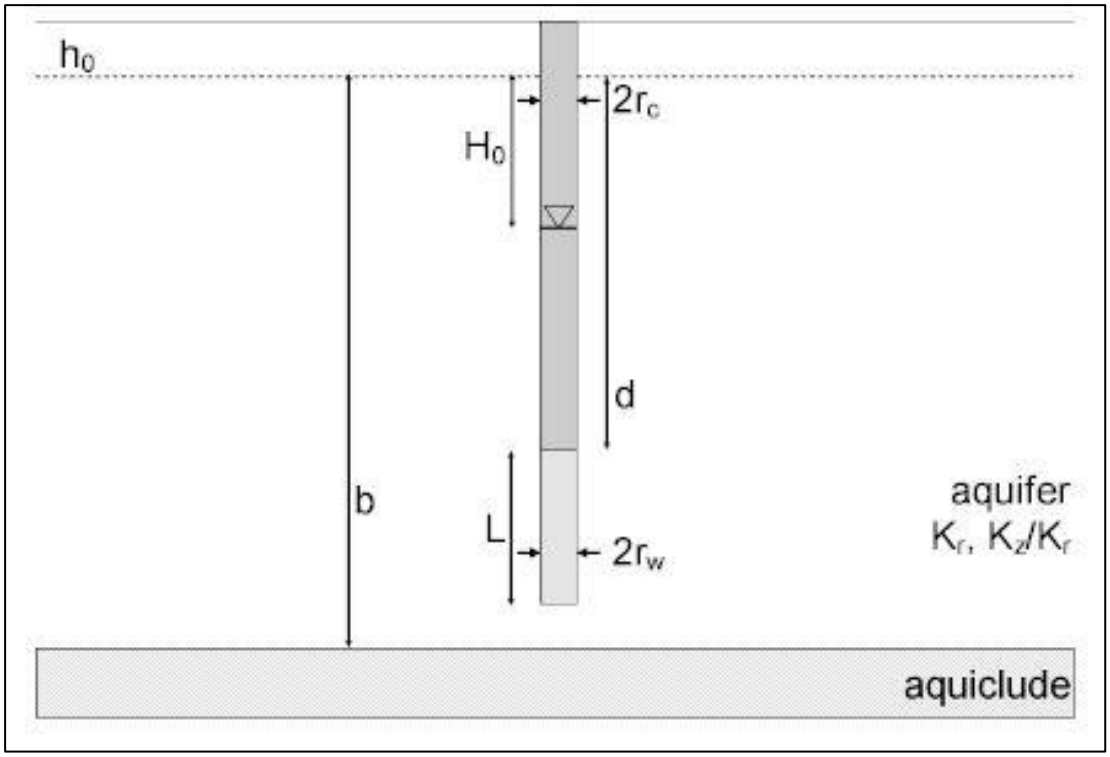

Figure 4-5: Piezometer geometry for Bouwer-Rice method (Bouwer and Rice 1976).

5.0 RESULTS AND DISCUSSION

Geological and hydrogeological data were collected to aid in the conceptualisation of the area. The analysed data were used to complement the data collected during the field trip. Field data collected from boreholes, quarries, and dams with results from the analysis are presented and discussed in this section.

5.1 HYDRAULIC PROPERTIES

The Bouwer-Rice (1976) method for interpreting slug test data was selected for use in the AQTESOLV software package. This method is ideal because it does not overestimate hydraulic conductivity compared to other methods, it also provides estimates within 30 % of actual field values. Two slug tests were performed, one at BH01- shallow well and the other at BH02 deep well. BH03 could not be tested as it was collapsed and was only able to equip the hole after the field visit was concluded. From the results presented below, the calculated hydraulic conductivities are 0.014 m/day and 0.033 m/day for boreholes BH01 and BH02, respectively. The calculated transmissivities are 0.44 m^2/day and 1.19 m^2/day for boreholes BH01 and BH02, respectively. A change in configuration for both displacement curves was noted. The change in configuration is likely due to the well construction i.e. “skin effects”, therefore, the first readings would indicate a lag time where measurements are from gravel packs. Input parameters and the results from the calculations are presented in Table 5-1, Figure 5-1 and Figure 5-2. The full dataset is attached as Appendix 4.

Table 5-1: Input parameters for AQTESOLV software.

Item	Input		Description
Borehole	BH01	BH02	-
SWL	18.75	13.79	Static Water Level (mbgs)
Vs (*l*)	1.9	1.9	Volume of Slug (*l*)
Ac (m^2)	0.003117	0.003117	Area of casing (m^2)
h_0	0.61	0.61	Observed initial displacement (Change in water level from static) (m)
L (m)	8.7	8.7	Length of screen (m)
dc (m)	0.063	0.063	Diameter of casing (m)
D (m)	0.1651	0.1651	Diameter of Well (m)
Saturated thickness (m)	31.25	36.21	Saturated thickness of the aquifer

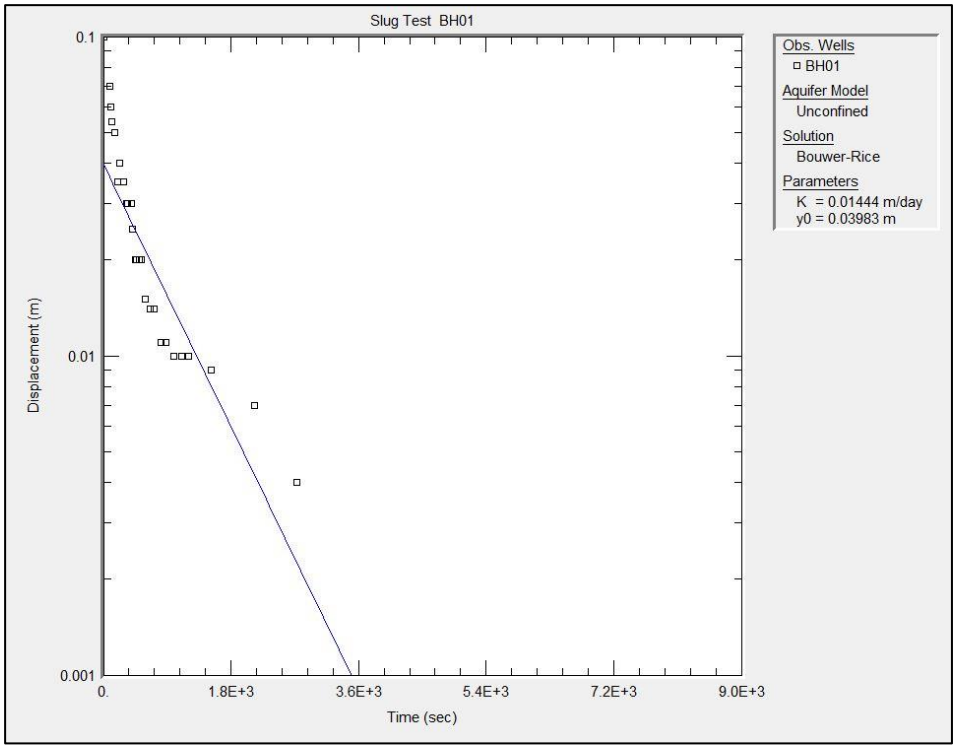

Figure 5-1: Slug test results from BH01.

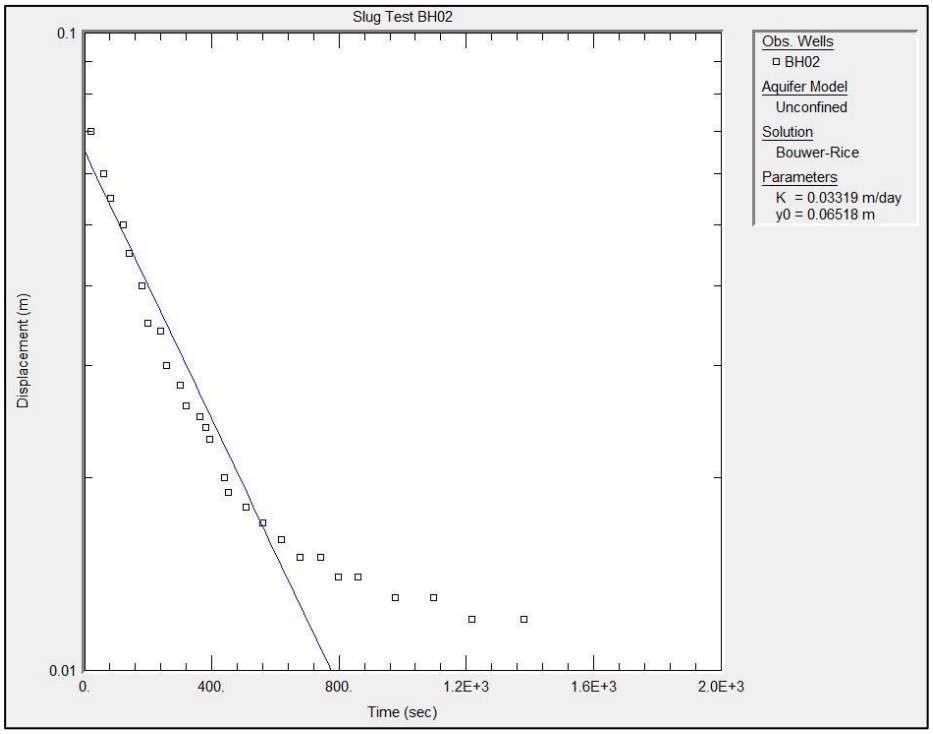

Figure 5-2. Slug test results from BH02.

5.2 HYDROCHEMISTRY

The water chemistry results presented in this section are from different sampling campaigns. The water chemistry results provided by the factory are merged with the water chemistry results collected during the fieldwork for this study. Table 5-2 presents the error percentage of ions, the full table showing all the results is presented in Appendix 5 in this report.

Table 5-2: Error percentage of ions of the results from the laboratory.

Sample ID	% Accuracy
IAL 1	-5.6
IAL 2	-0.05
IAL 3	0.26
IAL 4	2.2
IAL 5	8.7
IAL 7	-1.2

5.2.1 Groundwater Chemistry

5.2.1.1 Major Ion Chemistry

Major ions in the groundwater were detected in the following order: HCO_3^- > Na^+ > SO_4^{2-} > Ca^{2+} > Mg^{2+} > K^+ > Cl^- > F^-. Figure 5-3 shows that the pH for groundwater samples ranges from 7.4 to 8, which is the range normally observed in natural groundwaters. Table 5-3 shows the descriptive statistics for major ions detected in the groundwater system during the field campaign undertaken in 2018.

Table 5-3: Ions detected in the groundwater system during the field campaign with statistical analysis.

Sample ID	pH	EC µS/cm	TDS mg/l	Ca^{2+} mg/l	Mg^{2+} mg/l	Na^+ mg/l	K^+ mg/l	Cl^- mg/l	SO_4^{2-} mg/l	F^- mg/l	HCO_3^- mg/l
IAL 1	7.7	459.0	270.0	37.0	9.7	42.0	4.3	11.5	81.0	0.3	156.0
IAL 2	7.9	215.9	136.0	14.4	4.8	21.0	4.3	2.9	21.0	0.3	81.0
IAL 3	7.9	229.5	142.0	14.3	6.5	24.0	3.9	2.7	11.0	0.3	104.0
IAL 4	7.4	381.0	162.0	11.3	10.3	43.0	9.3	8.7	32.0	0.1	123.0
IAL 5	7.7	363.0	184.0	11.4	10.3	42.0	10.7	10.0	34.0	0.1	98.0
IAL 7	8.0	170.5	88.0	17.1	4.9	11.7	1.6	0.1	2.6	0.5	90.0
Min	7.4	170.5	88.0	11.3	4.8	11.7	1.6	0.1	2.6	0.1	81.0
Max	8.0	459.0	270.0	37.0	10.3	43.0	10.7	11.5	81.0	0.5	156.0

Sample ID	pH	EC µS/cm	TDS mg/l	Ca^{2+} mg/l	Mg^{2+} mg/l	Na^{+} mg/l	K^{+} mg/l	Cl^{-} mg/l	SO_4^{2-} mg/l	F^{-} mg/l	HCO_3^{-} mg/l
Arithmetic mean	7.8	303.2	163.7	17.6	7.7	30.6	5.7	6.0	30.3	0.3	108.7
Std deviation	0.2	103.7	55.8	8.9	2.4	12.3	3.2	4.3	25.2	0.2	24.8

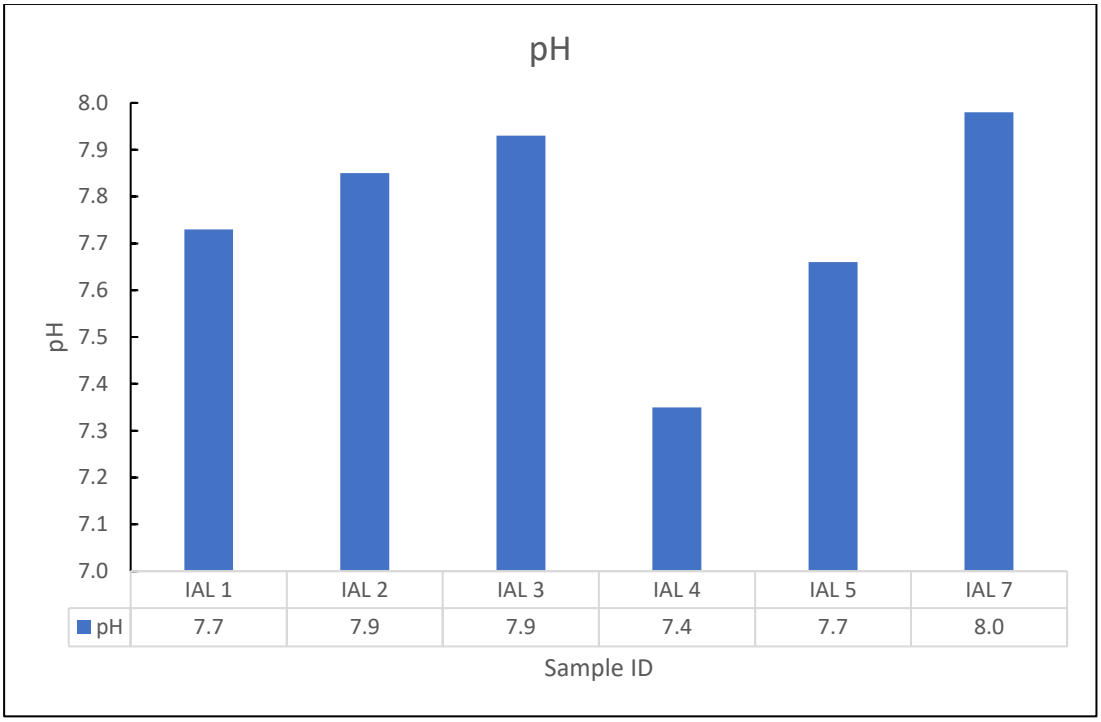

Figure 5-3: pH values for groundwater samples at Corobrik Glencoe Factory site.

The correlation coefficient (R) is used in this study to establish relationships of ions and their dependability on one another. For this study, R > 0.5 is considered a strong correlation, while R < 0.5 is considered a weak correlation. From Table 5-4, strong correlations (R > 0.8) exist for EC with Mg^{2+}, Na^{+}, Cl^{-}, SO_4^{2-}, and HCO_3^{-}, this suggests that these parameters are significant in the mineralisation of groundwater in the study area. Ca^{2+} and Mg^{2+} have a weak correlation (R = 0.16). This suggests that these ions do not have a common source. K^{+} shows weak correlations with most of the parameters, suggesting that this ion mostly originates from K^{+} bearing rocks (K-

feldspars). Table 5-4 shows the correlation matrix for groundwater hydrochemical paraments detected in the groundwater system.

Table 5-4: Correlations matrix between physiochemical variables (n = 6).

	EC µS/cm	TDS mg/l	Ca^{2+} mg/l	Mg^{2+} mg/l	Na^{+} mg/l	K^{+} mg/l	Cl^{-} mg/l	SO_4^{2-} mg/l	F^{-} mg/l	HCO_3^{-} mg/l
EC µS/cm	1.00									
TDS mg/l	0.91	1.00								
Ca^{2+} mg/l	0.50	0.72	1.00							
Mg^{2+} mg/l	0.92	0.71	0.16	1.00						
Na^{+} mg/l	0.95	0.79	0.20	0.97	1.00					
K^{+} mg/l	0.58	0.32	-0.39	0.80	0.80	1.00				
Cl^{-} mg/l	0.98	0.89	0.39	0.93	0.97	0.69	1.00			
SO_4^{2-} mg/l	0.90	0.98	0.78	0.66	0.74	0.24	0.86	1.00		
F^{-} mg/l	-0.62	-0.37	0.36	-0.80	-0.83	-0.98	-0.71	-0.29	1.00	
HCO_3^{-} mg/l	0.85	0.85	0.76	0.67	0.68	0.12	0.74	0.87	-0.20	1.00

Figure 5-4 shows the EC measured on-site, together with the TDS. From the figure, all the samples show an EC value of below 1500 µS/cm, with values ranging from 170 µS/cm to 459 µS/cm. The TDS concentrations are also low, implying that the water has low salinity. The EC and TDS values indicate fresh groundwater of low salinity. Figure 5-4 also shows that TDS for groundwater samples coincides with EC values, having exceptionally low concentrations below 1000 mg/l and thus the water is classified as freshwater with the highest TDS concentration measuring just 270 mg/l.

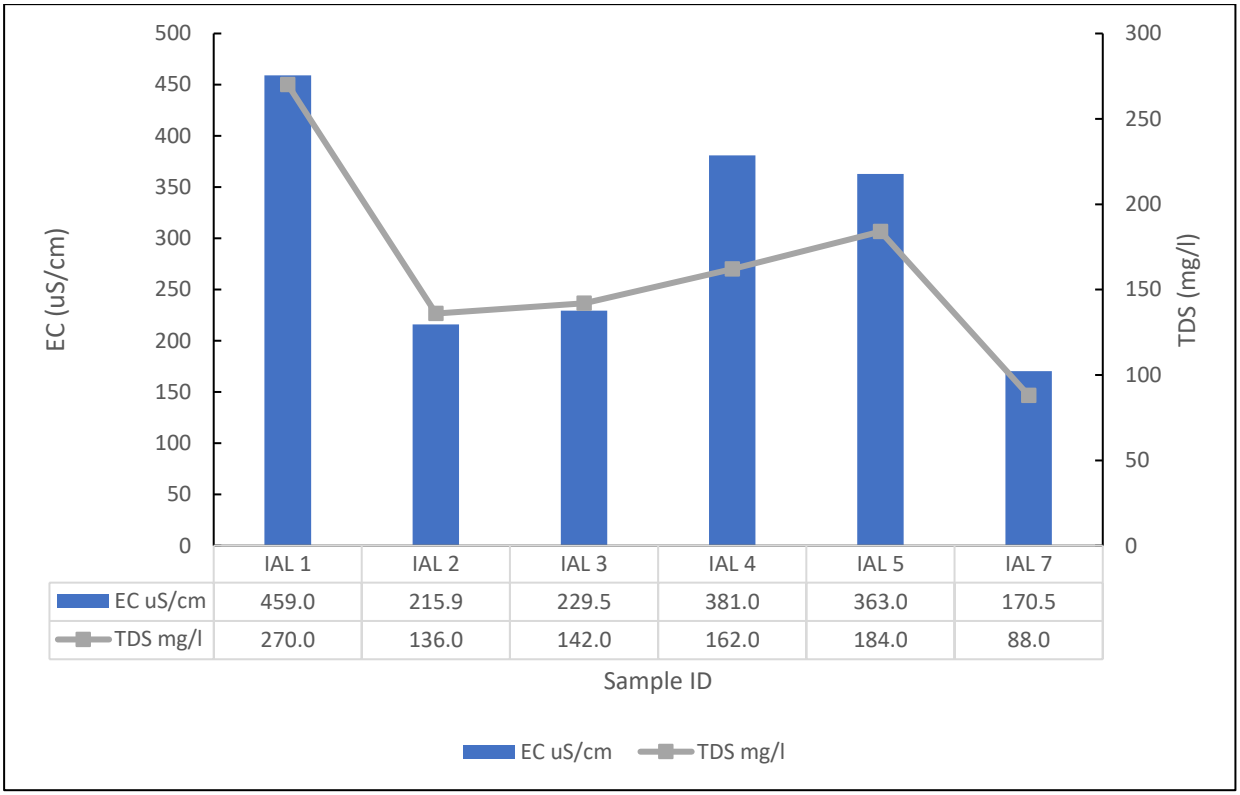

Figure 5-4: EC and TDS values for groundwater samples at Corobrik Glencoe Factory site

Figure 5-5 and Figure 5-6 shows a plot of anions and cations, respectively. The dominant anion in the groundwater is HCO_3^- measuring 156 mg/l for borehole IAL 1. Most of the concentrations of the anions fall just under 100 mg/l. The sulphate concentration for the current groundwater system is low with the highest concentration being just over 80 mg/l. The chloride concentration is the lowest in the analysed samples with the highest concentration being just 11 mg/l. The plot in Figure 5-6, shows that Na^+ concentration is the highest from the cation category, followed by Ca^{2+}. K^+ concentration is the lowest with concentrations measuring just 10.7 mg/l as the highest from all the samples. From the two plots, it is evident that bicarbonate dominates the groundwater system, the low concentrations of bicarbonate in the system could possibly be derived from carbonic acid from rainfall and contained in the soils.

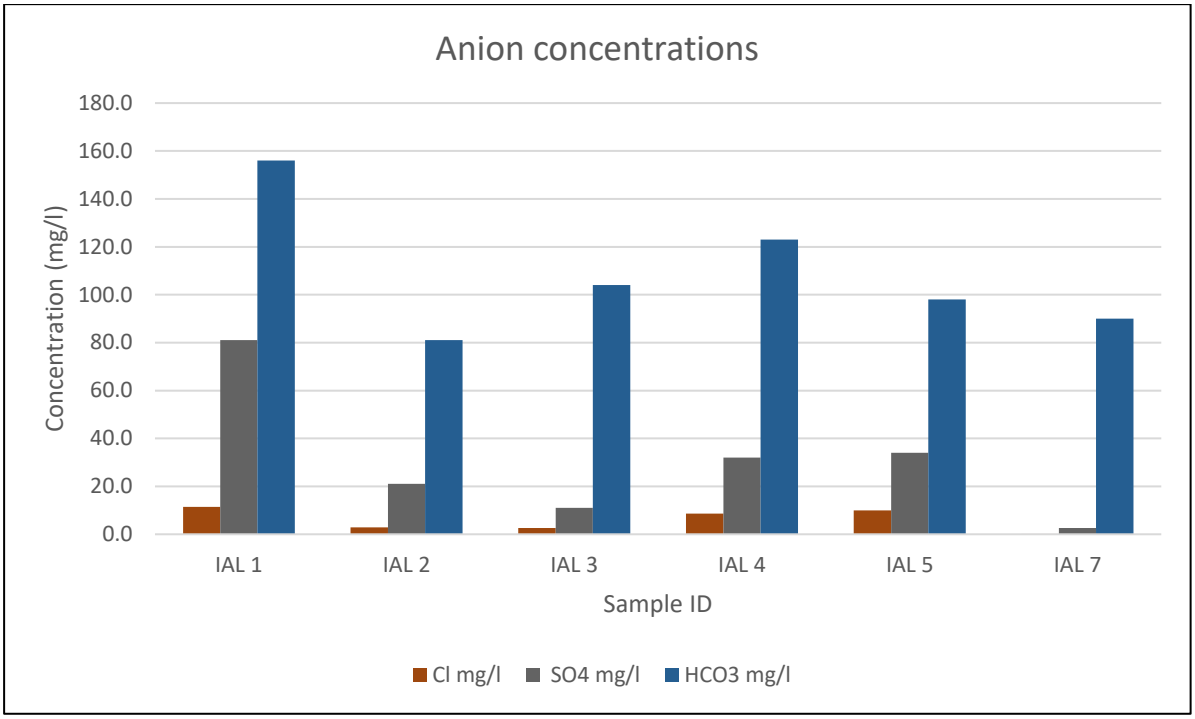

Figure 5-5: Anion values for groundwater samples at Corobrik Glencoe Factory site.

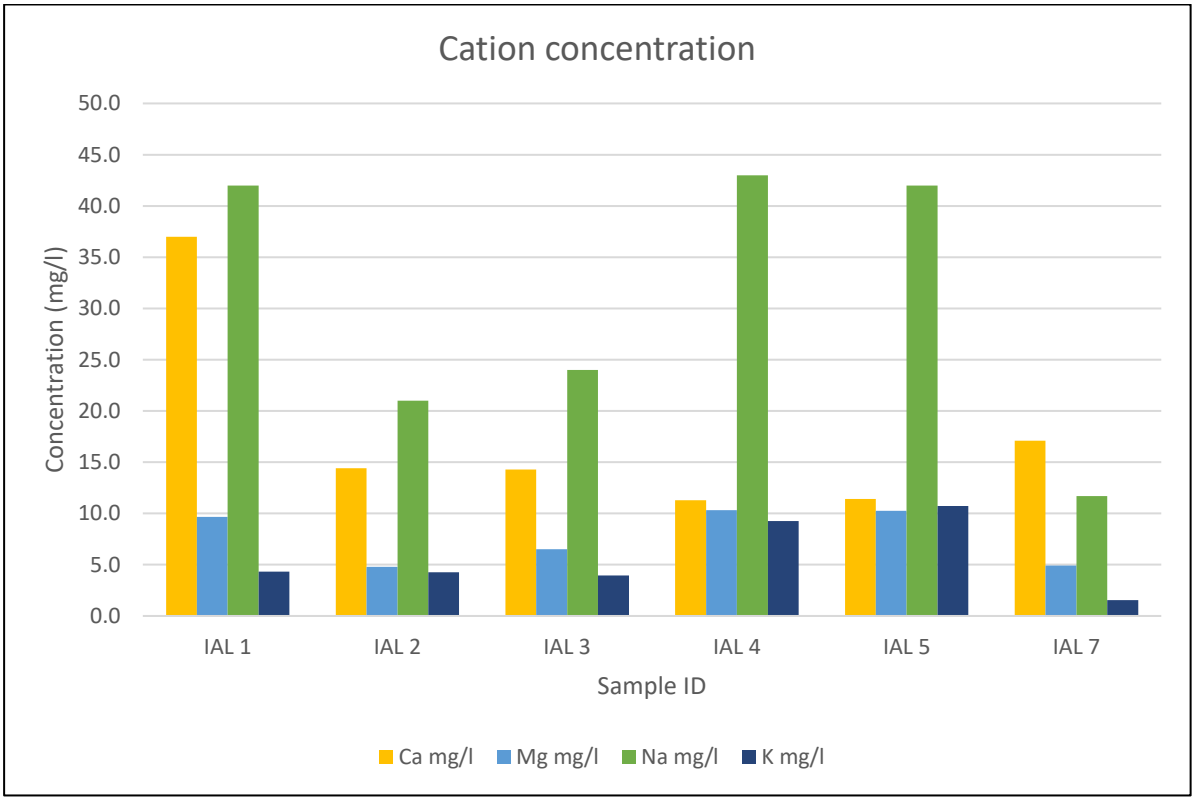

Figure 5-6: Cation values for groundwater samples at Corobrik Glencoe Factory site.

5.2.1.2 Water Types

Analyses of multiple parameters are further represented graphically using a piper diagram to identify water types. In the present study, a piper diagram identified two main water types for the groundwater system. From the piper diagram (Figure 5-7), two dominant water types are identified and discussed below:

1. Ca^{2+}- HCO_3^- water type

   This water type is characterised as freshwater due to low levels of Cl^-. The TDS of this cluster is below 1000 mg/l further confirming that this is freshwater. Sample IAL 1 showed the highest SO_4^{2-} concentration (81 mg/L). This sample has the highest TDS value of 270 mg/l with a high EC value of 459 µS/cm. Water hardness was calculated, and the results are presented in Table 5-5, which indicates that sample IAL 1 is categorised as moderately hard (132.1 mg/l as $CaCO_3$).

2. Na^+- HCO_3^- water type

   The HCO_3^- concentration in this water type is generally high, e.g. samples IAL 4 and IAL 5 showed levels of 123 mg/L and 98 mg/L, respectively. Because the ion exchange process might have removed Ca^{2+} (Hiscock, 2005), these water types are soft with a total hardness of 70 mg/l as $CaCO_3$; see Table 5-5 for water hardness for the groundwater in the study area.

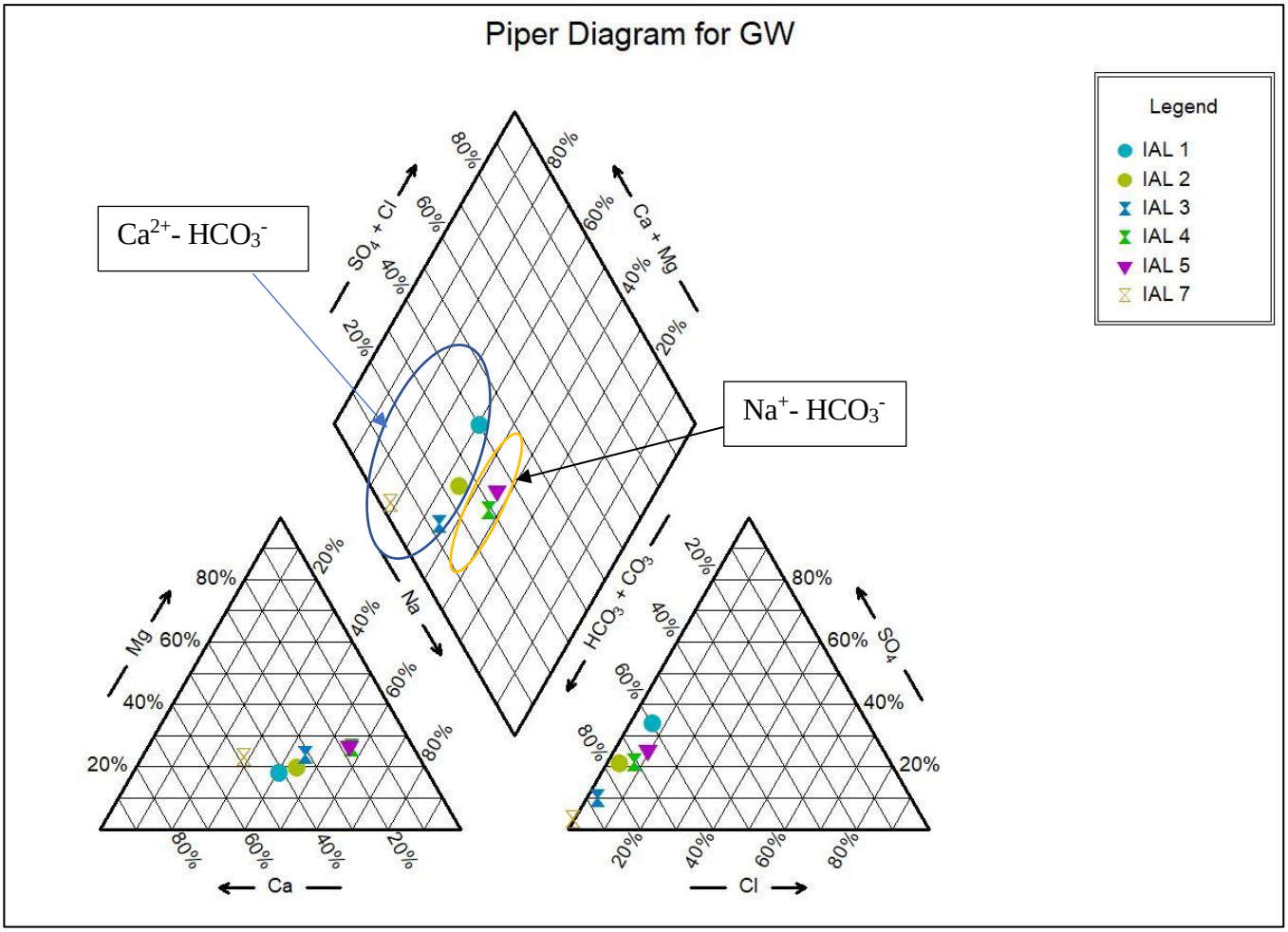

Figure 5-7: Piper diagram for groundwater samples collected in the study area.

Table 5-5: Groundwater hardness for the study area.

Sample ID	Source	Mg^{2+}	Ca^{2+}	$4.1*Mg^{2+}$	$2.5*Ca^{2+}$	Total Hardness	Classification
IAL 1	Ground Water	9.66	37	39.606	92.5	132.106	moderately hard
IAL 2	Ground Water	4.8	14.4	19.68	36	55.68	soft
IAL 3	Ground Water	6.52	14.3	26.732	35.75	62.482	soft
IAL 4	Ground Water	10.31	11.3	42.271	28.25	70.521	soft
IAL 5	Ground Water	10.26	11.4	42.066	28.5	70.566	soft
IAL 7	Ground Water	4.93	17.1	20.213	42.75	62.963	soft

5.2.1.3 Processes Influencing Water Chemistry

Although it is identified that two groundwater types exist, the samples appear to be clustered together and could indicate a possibility of ion exchange of Ca^{2+} by Na^{+} and water type changes from Ca^{2+}- HCO_3^{-} water type to the Na^{+}- HCO_3^{-} water type. To confirm this, this process has been investigated using the Durov diagram. The Durov diagram displays possible geochemical processes that may be influencing the system and can show ion exchange, reverse ion exchange and mixing of different water types (Aly *et al*., 2014). Figure 5-8 shows a Durov diagram for both groundwater and surface water for the current study. Groundwater samples plot in field 2, this field is dominated by Ca^{2+} and HCO_3^{-}, according to Salman *et al* (2013) samples in this field with substantial Na^{+} are presumed to represent ion exchange of Ca^{2+} for Na^{+}. It has already been shown that Na^{+} is significant in the current groundwater system (Figure 5-6). Two groundwater samples (IAL 4 and IAL 5) plot in field 3, field 3 is water that is dominated by Na^{+} and HCO_3^{-} and this field also indicates ion exchange processes (Salman *et al*., 2013).

From Figure 5-8, surface water samples are clustered in field 2, these samples here indicate the influence of SO_4^{2-} on the water and this is consistent with the surface water piper diagram (Figure 5-15). Surface water samples in field 1 indicate a recent recharge of Ca^{2+}- HCO_3^{-} water (Dlamini and Demlie, 2020).

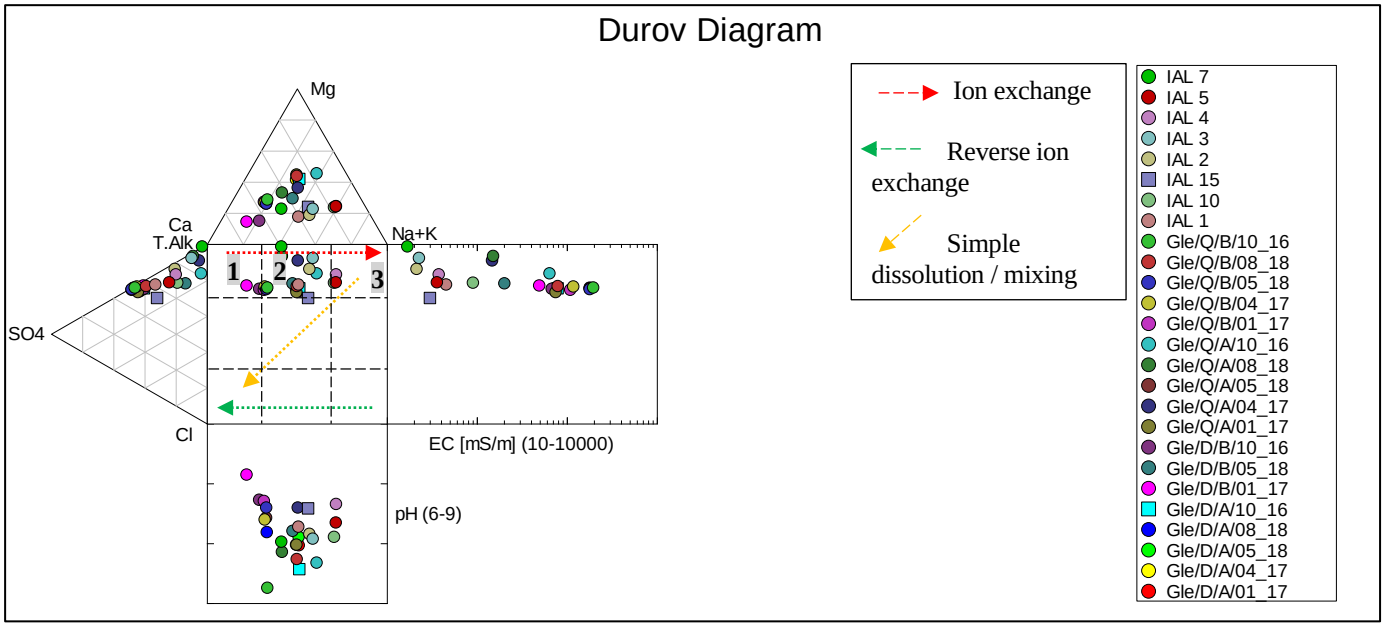

Figure 5-8: Durov Diagram of water samples collected in the study area.

Figure 5-9 and Figure 5-10 show the Gibbs diagram which provides further evidence of water-rock interaction (weathering) as the process controlling the groundwater mineralisation. The scatter of $Na^+/(Na^+ + Ca^{2+})$ values from low to high without significant variations in TDS also suggests that cation exchange influences the chemical compositions by increasing Na^+ and decreasing Ca^{2+} (Huang *et al*, 2018). The low ratio of Cl^-: $Cl^- + HCO_3^-$ plotted against TDS corresponds to the low salinity levels that are observed in the current groundwater system (Ghesquière *et al*., 2015).

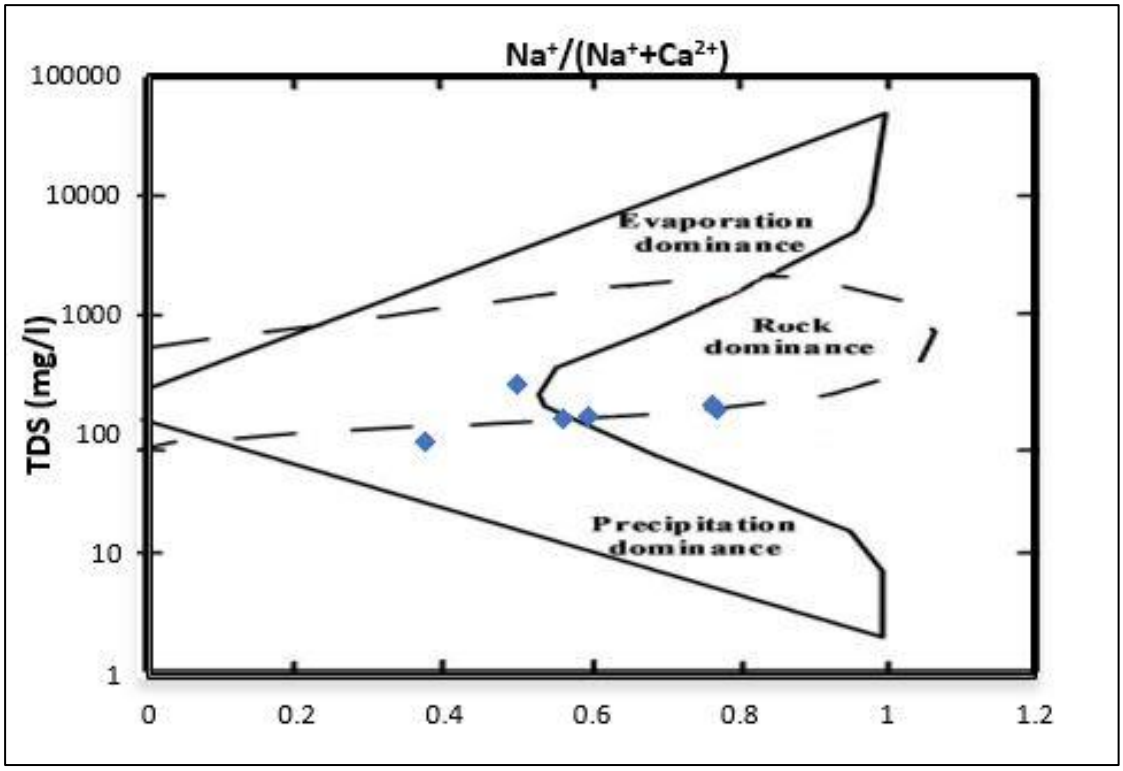

Figure 5-9: Gibbs diagram highlighting the processes controlling groundwater mineralisation.

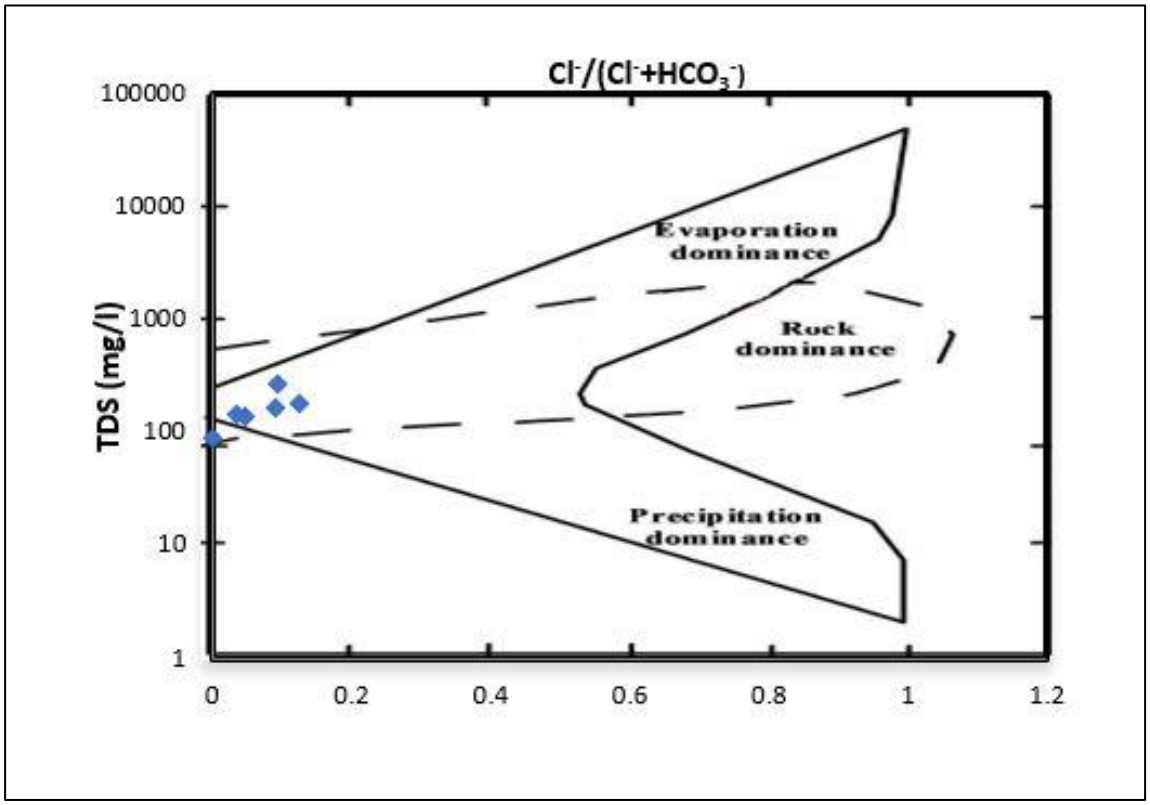

Figure 5-10: Gibbs diagram highlighting the processes controlling groundwater mineralisation.

The weathered aquifer within the study area is characterised by the sandstones of the Ecca Group where quartz is the dominant mineral. The approximate 1:1 increase (R=0.71) in total cations and alkalinity (Figure 5-11) of the groundwater samples suggests the dissolution of silicate minerals, more especially plagioclase, which may be from the dolerites in the area.

When Cl^- or SO_4^{2-} dissolution is responsible for water chemistry, the total cations (meq/l) vs Cl^- + SO_4^{2-} (Figure 5-12) concentrations are balanced i.e. total cations (meq/l) /(Cl^- + SO_4^{2-}) = 1. In the present groundwater system, the ratio is greater than 1. This is consistent with silicate minerals being responsible for the groundwater chemistry in the study area. The higher ratio also indicates that human activities might have a limited influence on groundwater chemistry in the current groundwater system (Huang *et al.*, 2018).

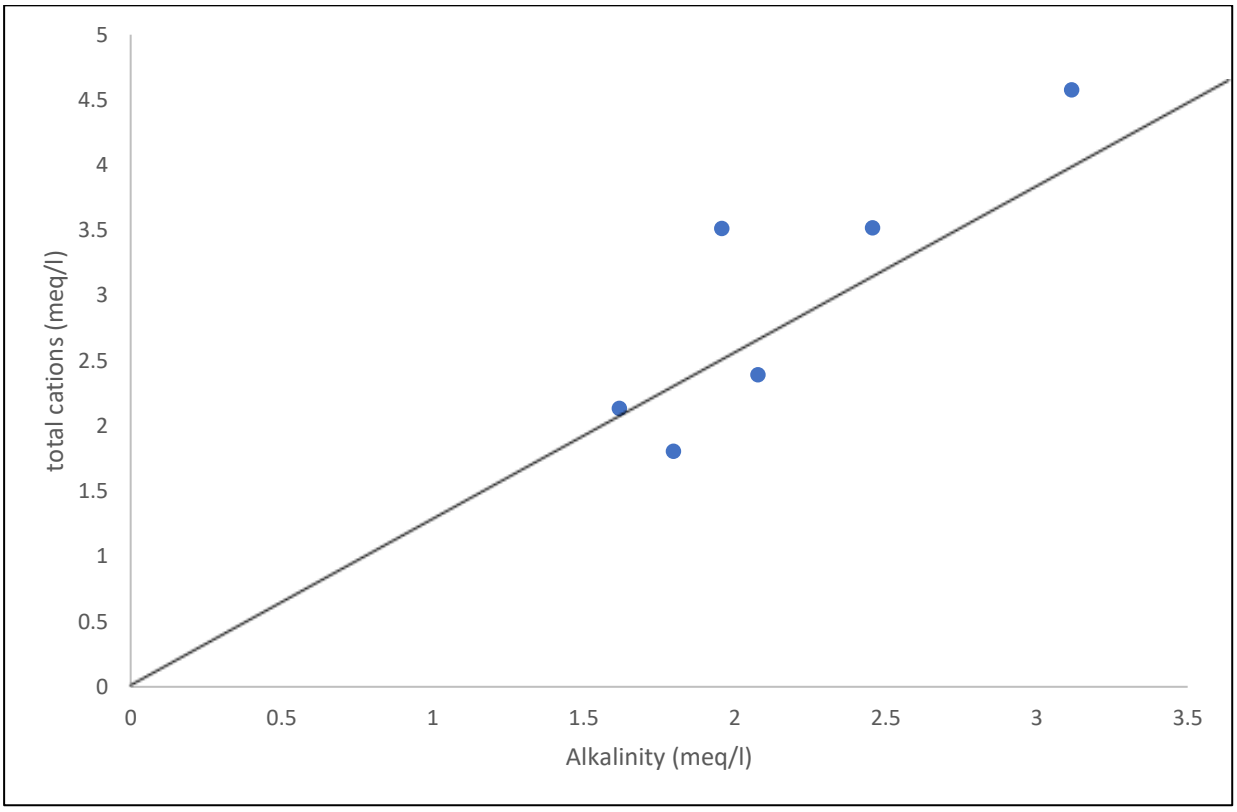

Figure 5-11: plot of total cations vs HCO_3^-.

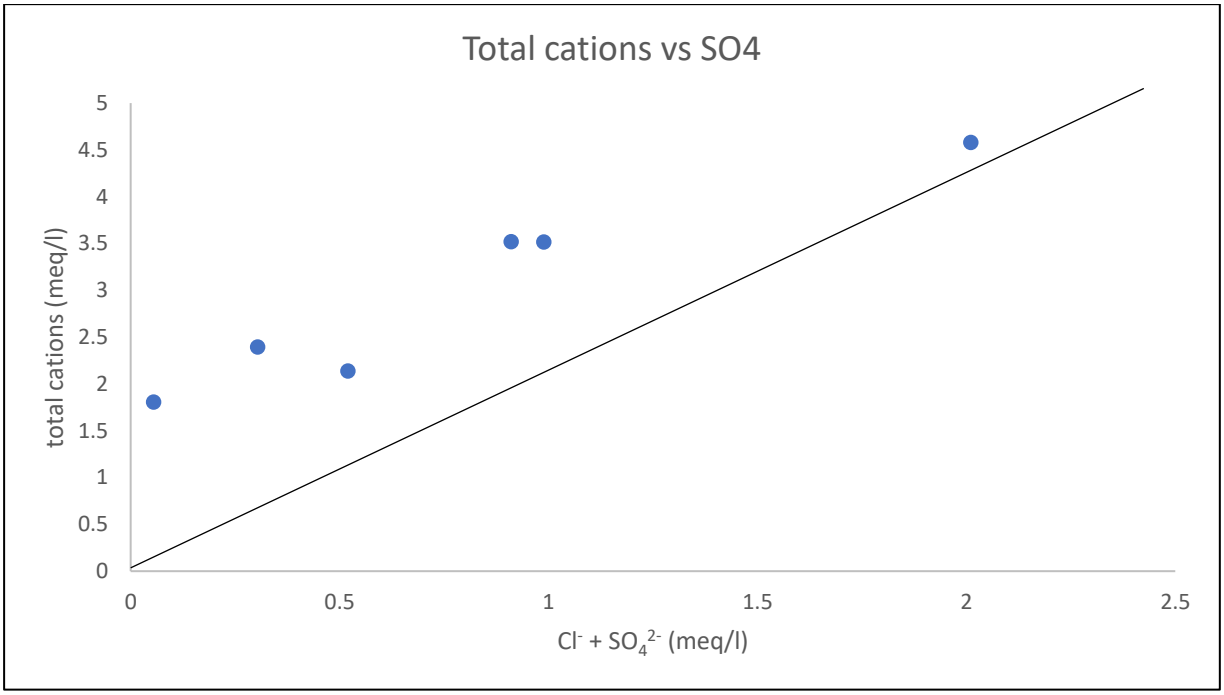

Figure 5-12: Plot of total cations vs $Cl^- + SO_4^{2-}$.

To further characterise the groundwater chemistry for the site, Stiff diagrams and XY scatter plots are used. Figure 5-13 shows the stiff diagrams while the XY scatter plot is presented in Figure 5-14.

Further assessments using the stiff diagram, Figure 5-13, showed that the presence of bicarbonates influences the groundwater samples. Nadiri *et al*. (2013) used stiff diagrams to classify groundwater from different origins. Water that had high bicarbonate concentration coupled with high Ca^{2+} and Mg^{2+} or high Ca^{2+} were classified to originate from dolomites and limestone, respectively. From the current study, samples do not show an obvious water origin/source as described by Nadiri *et al*. (2013). However, it is evident that samples IAL 4 and IAL 5 originate from the same source while other samples could likely be from different sources.

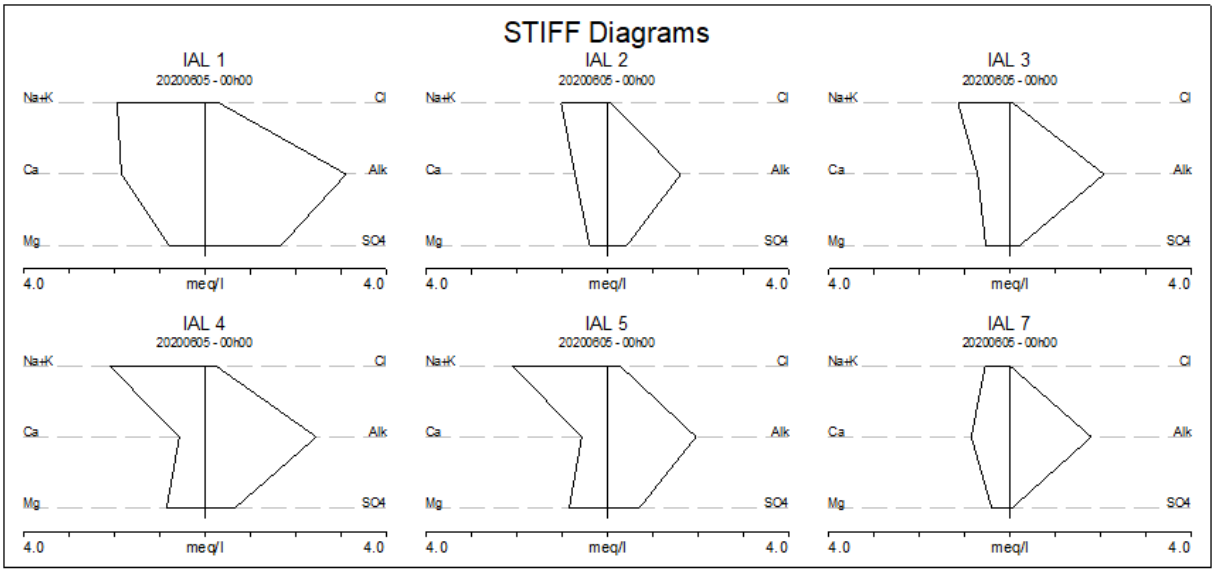

Figure 5-13: Stiff diagram for groundwater samples collected in the study area.

The XY scatter plots are used to define relationships between ions. Gomo and Vermeulen (2014) used a plot of Ca^{2+} and Mg^{2+} vs SO_4^{2-} to show that in a groundwater system influenced by AMD, SO_4^{2-} should increase linearly and simultaneously with Ca^{2+} and Mg^{2+}. Concentrations measured in the current groundwater system did not increase linearly at the same time. The R^2 value is 0.43 and 0.61 for Mg^{2+} and Ca^{2+}, respectively. No positive correlation exists between SO_4^{2-} and Mg^{2+}; however, such correlation exists only for Ca^{2+}. This is interpreted as Ca^{2+} increases linearly at the same time with SO_4^{2-} (Figure 5-14). The lack of a linear increase of the three ions together, according to Gomo and Vermeulen (2014), suggests that AMD does not influence the groundwater system. Gomo and Vermeulen (2014) further used stoichiometry based on the slopes of the scatter plots to show how a groundwater system that is affected by AMD behaves. They showed that in an AMD influenced groundwater system, the SO_4^{2-} vs Ca^{2+} and SO_4^{2-} vs Mg^{2+} plots should have slopes of 1.3 and 4, respectively. Field data for the current groundwater system (Figure 5-14) shows that the plot of SO_4^{2-} vs Ca^{2+} and SO_4^{2-} vs Mg^{2+} are characterised by slopes of 0.9 and 1.7, respectively, which is not close to the prediction. This is interpreted as a piece of evidence that AMD does not influence the current groundwater system. This observation is consistent with the plot of total cations vs $Cl^- + SO_4^{2-}$ (Figure 5-12), where it was observed that the chemical composition of the groundwater system in the area is not influenced by human activities.

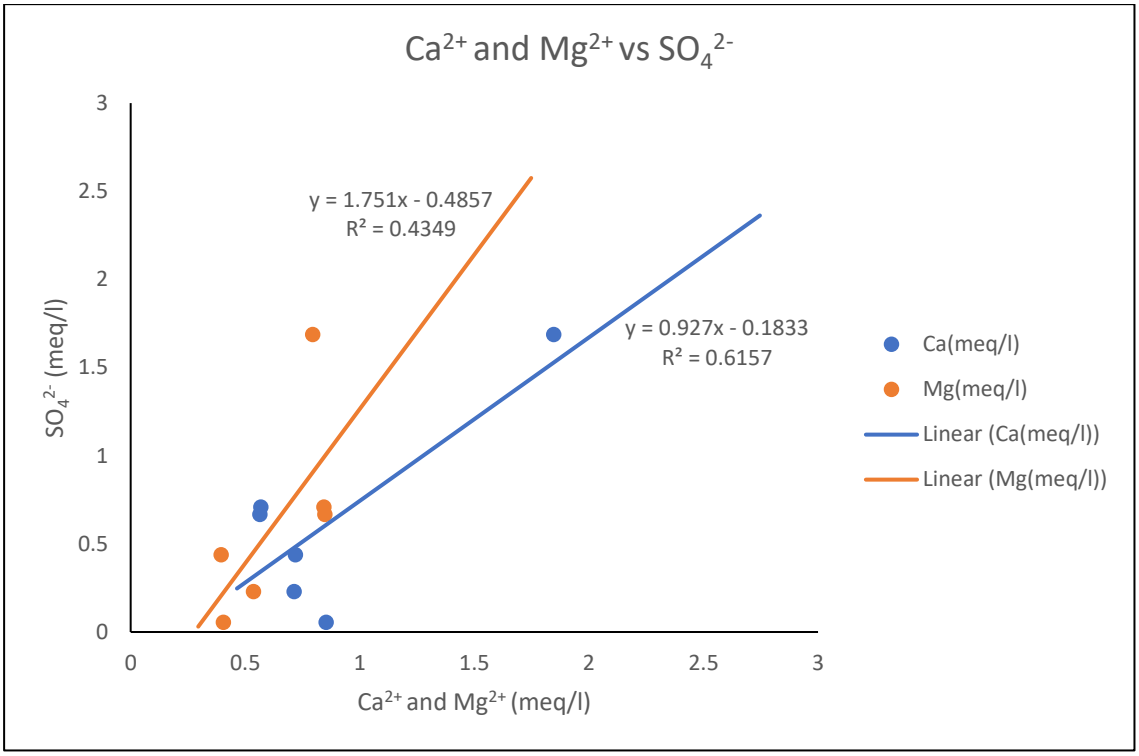

Figure 5-14: Scatter plot showing SO_4^{2-} vs Ca^{2+} and Mg^{2+} concentrations for the study area.

5.2.1.4 Metals

Pollution of natural watercourses in mine areas is common; the mine drainage often contains high concentrations of metals and metalloids which are toxic to the groundwater and surface waters in mine areas (Halim *et al*, 2012). Pyrite is the most common mineral in coal deposits; it occurs with metals such as Hg, Co, Cd, Cu, Bi, Mo, Zn, Re, Sn and Pb (Gomo & Vermeulen, 2014). Metals have the potential to leach from rocks into water under acidic conditions, which prevail in AMD influenced system. It is vital to measure these concentrations and assess the levels of metal concentrations in the groundwater and surface waters. Metal analysis was performed on groundwater and surface water in this study. Table 5-6 shows the descriptive statistics of the analysed data, the full results are presented as appendix 5. The data are compared with results obtained by Gomo and Vermeulen (2014), and it is observed that the mean concentrations for most metals in the current study are above the concentrations obtained by Gomo and Vermeulen (2014). These include Ba, Cr, Fe, Cu, Bo, and Mn. From the appendix, however, it is noted that these concentrations were not above the guideline limits of regulatory bodies including SANS and WHO. Most concentrations are considered to be background concentrations of groundwater derived from rocks. Exceptions may exist for Fe, Mn, Al, and Cr. The highest concentrations for

these metals were recorded at sampling locations IAL 2 and IAL 3, which is one borehole equipped with shallow and deep PVC pipes, respectively. This borehole is the furthest away from the surface footprint of the old mines and the source of these metals is unlikely from the surface operations. From Figure 3-2 it is noted that old underground operations are said to have existed at this location, therefore the source might be from oxidation of the pyrite in the vadose zone.

Table 5-6: Descriptive statistics of the metal concentration in the study area. Also shown is the average concentrations from another study for comparison.

Parameter	Minimum (mg/l)	Maximum (mg/l)	Arithmetic mean (mg/l)	Arithmetic mean (mg/l) (Gomo and Vermeulen, 2014)	Std Deviation (mg/l)
Silver as Ag mg/l	0.004	0.004	0.004	*np	0
Aluminium as Al mg/l	0.14	40	11.15333	*np	15.04206
Arsenic as As mg/l	0.001	0.001	0.001	*np	0
Boron as B mg/l	0.006	0.064	0.016667	0.115	0.021281
Barium as Ba mg/l	0.001	0.62	0.258833	0.039	0.257544
Beryllium as Be mg/l	0.002	0.002	0.002	0.004	0
Bismuth as Bi mg/l	0.005	0.005	0.005	*np	0
Cadmium as Cd mg/l	0.001	0.001	0.001	0.004	0
Cobalt as Co mg/l	0.001	0.061	0.013833	0	0.021497
Chromium as Cr mg/l	0.003	0.25	0.058667	0.009	0.087857
Copper as Cu mg/l	0.004	0.18	0.054167	0.012	0.058806
Iron as Fe mg/l	0.34	84	22.12	4.93	28.79527
Manganese as Mn mg/l	0.015	1.75	0.4415	0.86	0.602566
Molybdenum as Mo mg/l	0.001	0.001	0.001	0.003	0
Nickel as Ni mg/l	0.003	0.1	0.026833	0.014	0.034883
Lead as Pb mg/l	0.003	0.076	0.024833	0.027	0.025926
Phosphorus as P mg/l	0.04	1.13	0.336167	*np	0.377717
Antimony as Sb mg/l	0.01	0.01	0.01	*np	0
Selenium as Se mg/l	0.001	0.001	0.001	*np	0
Tin as Sn mg/l	0.02	0.02	0.02	*np	0
Strontium as Sr mg/l	0.098	1.18	0.401333	3.708	0.378702
Titanium as Ti mg/l	0.001	0.35	0.077167	*np	0.125582
Thallium as Tl mg/l	0.009	0.009	0.009	*np	0
Uranium as U mg/l	0.004	0.004	0.004	*np	0
Vanadium as V mg/l	0.002	0.16	0.038333	0.122	0.056894
Zinc as Zn mg/l	0.005	0.21	0.048833	0.164	0.073345
Zirconium as Zr mg/l	0.001	0.021	0.006833	*np	0.007448
Thorium as Th mg/l	0.002	0.017	0.0045	*np	0.00559
Mercury as Hg mg/l	0.001	0.001	0.001	0	0

*np : not reported

5.2.2 Surface water Chemistry

The factory collects surface water samples for monitoring purposes. Data from the monitoring programme were made available for the years 2016 to 2018. These data were merged with two surface water samples collected during the fieldwork. The sample location for the samples described in this section are shown in Figure 4-3 and Table 5-7; the full results are attached as Appendix 6.

Table 5-7.: Surface samples collected by Corobrik Glencoe.

Sample Name	Location Sampled
GLE/D/A	Dam (Quarry 3)
GLE/D/B	Runoff Water from Workshop into Dams
GLE/Q/A	Quarry Next to Dam
GLE/Q/B	Quarry North West of Factory

It is important to note that the data collected by the factory did not report the HCO_3^- concentration. Total alkalinity as HCO_3^- was calculated from the reported bicarbonate alkalinity as $CaCO_3$ using the following formula (Waterboards, 2020).

Considering the following reaction:

$$CaCO_3 + H_2O + CO_2 \rightarrow Ca(HCO_3)_2$$

Noting that $CaCO_3$ has a molecular weight of 100 g/mol and the HCO_3^- anion has a molecular weight of 61 g/mol

Therefore each mol of $Ca(HCO_3)_2$ corresponds to one mol of $CaCO_3$ (100 g) and contains 2 x 61 g = 122 g of HCO_3^- and the conversion is as follows:

Bicarbonate Alkalinity as HCO_3^- (mg/L) = 1.22 *Bicarbonate Alkalinity as $CaCO_3$ (mg/L)

The descriptive statistics for major ions are presented in Table 5-8. The physicochemical parameters, including pH, TDS, and EC results are also presented. From the table, the minimum pH value is 6.86, while the maximum pH value 8.75. These pH values are in the same range as the groundwater pH values. The EC values for surface water range from 91.3 µS/cm to 1980 µS/cm, while TDS ranges from 92 mg/l to 1748 mg/l. TDS values above 1000 mg/l are considered as brackish water.

Major ions in the surface water are identified in the following order: HCO_3^- > SO_4^{2-} > Ca^{2+} > Na^+ > Mg^{2+} > Cl^- > K^+ > F^-.

Table 5-8: Results from the surface water chemistry with descriptive statistics of the major ions detected from the factory monitoring data. Two samples from the 2018 fieldwork (IAL 10 & IAL 15) are included.

	pH	EC µS/cm	TDS mg/l	Ca^{2+} mg/l	Mg^{2+} mg/l	Na^{+} mg/l	K^{+} mg/l	Cl^{-} mg/l	SO_4^{2-} mg/l	F^{-} mg/l	HCO_3^{-} mg/l
IAL 10	7.9	91.3	111	3.1	2.53	9.78	3.86	4.58	9.42	0.2	36
IAL 15	7.425	304.5	160	18.4	8.3	26	6.23	14.47	43	0.3	76
Gle/D/A/10_16	8.44	797	588	52.9	48.2	60.5	12	25	282	0.69	402.6
Gle/D/A/01_17	8.04	756	576	47.4	43	52.9	10.8	25	285	0.64	359.9
Gle/D/A/04_17	8.03	748	522	48	40.5	47.9	10.7	22.4	252	0.59	350.14
Gle/D/A/05_18	7.9	772	532	45.6	39.5	50	11.1	22	256	0.55	336.72
Gle/D/A/08_18	7.82	1810	1367	230	71.7	97.2	3.36	16.7	917	0.45	1060.18
Gle/D/B/10_16	7.28	686	526	97.9	13.8	35.1	6.35	24.3	259	0.98	368.44
Gle/D/B/01_17	6.86	498	376	77.4	9.41	16.5	4.31	11.5	212	0.55	306.22
Gle/D/B/05_18	7.8	204	132	15.3	7.2	13.2	3.89	12.7	15.2	0.2	82.96
Gle/Q/A/10_16	8.33	647	422	25.6	43.1	67.3	3.68	37.7	12.3	0.96	294.02
Gle/Q/A/01_17	8.03	757	582	44.5	43.1	45	10	24.3	293	0.68	352.58
Gle/Q/A/04_17	7.41	149	92	11	7.66	12.1	1.8	4.01	3.85	0.05	71.98
Gle/Q/A/05_18	7.58	1820	1572	241	69.7	101	4.27	18.8	948	0.28	1084.58
Gle/Q/A/08_18	8.15	153	93	14.6	6.99	8.95	2.17	1.6	7.46	0.468	79.3
Gle/Q/B/10_16	8.75	1980	1748	277	91.6	117	4.5	25.1	1099	0.32	1304.18
Gle/Q/B/01_17	7.3	1100	892	132	39.4	48.5	4.28	14.1	552	0.31	600.24
Gle/Q/B/04_17	7.61	1190	956	161	47.4	62.3	4.15	14.5	583	0.41	728.34
Gle/Q/B/05_18	7.41	1810	1552	231	66.8	97.3	4.09	18.8	950	0.28	1039.44
Gle/Q/B/08_18	8.27	799	508	48.4	45.5	49.4	11.1	19.9	246	0.845	375.76
Minimum	6.86	91.3	92	3.1	2.53	8.95	1.8	1.6	3.85	0.05	36
Maximum	8.75	1980	1748	277	91.6	117	12	37.7	1099	0.98	1304.18
Arithmetic Mean	7.81675	853.59	665.35	91.105	37.2695	50.8965	6.132	17.873	361.2615	0.48765	465.479
Std Deviation	0.449884	580.429	507.8523	86.40367	25.04242	31.74427	3.322631	8.403972	348.9168	0.250858	372.3883

The surface water samples are plotted on diagnostic plots to characterise the water type and define possible hydrochemical processes taking place. A Piper plot is presented in Figure 5-15.

One main water type is identified from the Piper diagram with two other water types. Ca^{2+}- HCO_3^- water type is the primary water type, Mg^{2+}- SO_4^{2-} and Na^+- HCO_3^- exist as minor water types:

1. Ca^{2+}- HCO_3^- water type

These samples have the highest concentration of bicarbonates with the major cations being Ca^{2+}. Most samples from Gle/Q/A including Gle/Q/A/10_16, Gle/Q/A/08_18 and Gle/Q/A/04_17 identified in this water type. These samples are the furthest from the ash dump, and it is expected that they plot in this freshwater quadrant. Samples from Gle/D/A also plot in this quadrant, and this is expected as the two sampling locations are not far from each other. It must be noted that samples from Gle/D/A plot further towards the Mg^{2+}- SO_4^{2-} water type. Although the dominant anion is still bicarbonates, these samples show a trend of moving from Ca^{2+}- HCO_3^- water type to the Mg^{2+}- SO_4^{2-} water type. This is assumed to be influenced by the coal dumps on site. Sample Gle/D/A/08_18 has concentrations two times more than Gle/D/A/05_18 for most ions, including bicarbonates and calcium. This increase within 3 months is unjustified and may be due to analytical error as there are no records of chemical inputs from the factory that could have contributed to this abnormal increase in concentrations. The TDS for this water type is classified as fresh, measuring below 1000 mg/l; this is with the exception of sample Gle/D/A/08_18.

2. Mg^{2+}- SO_4^{2-}

This water type is generally characterised by the AMD influenced water. In the current study, only samples Gle/Q/B plots in this field. The samples show an evolving trend from Ca^{2+}- HCO_3^- water type. These samples provide the probability of some interaction with the minerals from the coal ash dumps as they are located near the ash dump. These samples have a TDS above 1200 mg/l and are classified as brackish water. Further classification of the ash dump and soils would be required to assess if the ash dump is releasing any contaminants to the soil and to the surface water.

3. Na^+- HCO_3^-

High sodium concentrations and bicarbonates characterise sample IAL 10. This sample is from a dam north-east of the coal ash dumps. This is the furthest sample from the visible operations on the ground and lacks SO_4^{2-}.

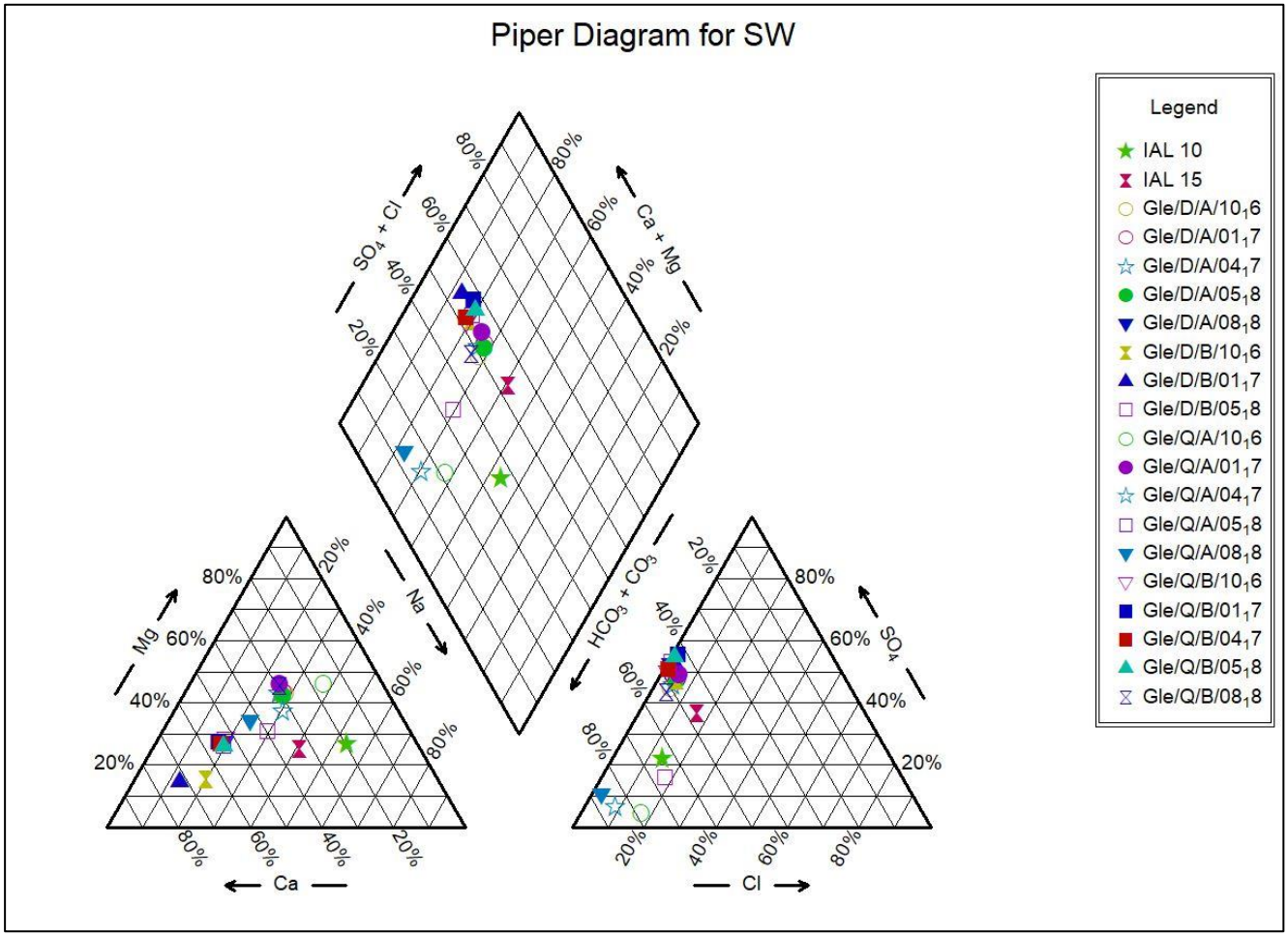

Figure 5-15: Piper diagram for surface water samples collected in the study area.

5.2.3 Groundwater and Surface water interaction

The groundwater and surface water chemistry have been discussed in the previous two subsections, this subsection presents Figure 5-16 which shows a common piper plot for both groundwater and surface water to assess any relationship between the two systems. From Figure 5-16, it is noted that two main clusters exist, C1 and C2. C1 is mainly surface waters and the water type is more inclined towards Mg^{2+}- SO_4^{2-} type. C2 is mainly groundwater and it is inclined towards the Na^{+}- HCO_3^{-} water type. There seems to be a distinct variation in the water chemistry for the two systems, suggesting that the surface water chemistry has minimal influence on the groundwater chemistry.

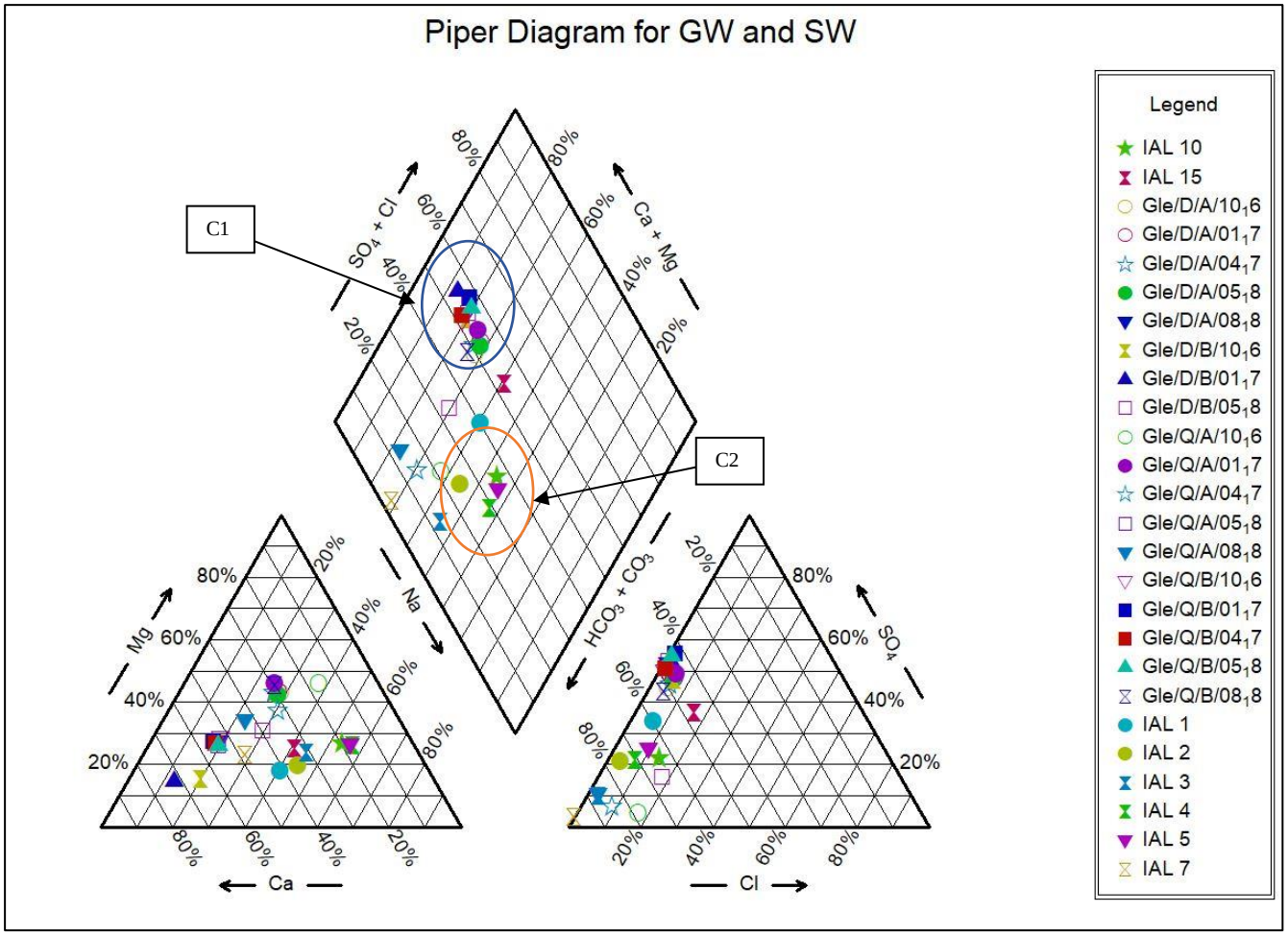

Figure 5-16: Piper plot incorporating both groundwater and surface water for comparison.

5.3 ENVIRONMENTAL ISOTOPES

Clark and Fritz (1997) stated that the stable isotopic composition of water is affected by processes, which can be studied to help in defining the origin of the water. Samples at the Corobrik site were taken for the analysis of the stable isotopes of oxygen – 18 and deuterium and the results are presented in Table 5-9. Groundwater and surface water isotopic results are plotted against the Global Meteoric Water Line (GMWL) and the Local Meteoric Water Line (LMWL) for comparison. The slope of LMWL is lower than the GMWL, according to Li *et al* (2020), this suggests that the low humidity condition dominates in the formation of rainfall.

Variations in isotopic compositions for groundwater and surface water are observed from Figure 5-17. This suggests that the groundwater and surface water contain isotopically different water which could be linked to different sources and hence the current surface water does not show a direct link with the groundwater.

The surface water samples include water from dams and quarries. The surface water isotope composition for $\delta^{18}O$ ranges from 0.61‰ to 6.64‰ and 6.9‰ to 36.8‰ for δD. Surface waters showed a more enriched isotopic signal plotting below the GMWL and LMWL, indicating the effect of evaporation with an evaporation regression of 0.98 and an equation of $\delta D = 4.31\ \delta^{18}O+7‰$. According to Kshetrimayum and Laishram (2020), the point of intersection for the evaporation line and GMWL is the original isotopic composition of the water before evaporation and is represented by a red circle ($0.9\delta^{18}O$ and 3.8 δD) in Figure 5-17.

Seven groundwater samples were analysed, and they all showed a highly depleted isotopic composition. The isotope composition for $\delta^{18}O$ ranges from -4.24‰ to -3.47‰ and -18.2‰ to -9.3‰ for δD. Groundwater samples plot above the GMWL and also plots above and on the LMWL. Samples that plot above the meteoric water line indicate a rainfall originated from high humidity (condensation) process, this included samples IAL 5 and IAL 6 within the existing boreholes found on site. The results from the isotope analyses of these two samples indicate that the water was derived from recent rainfall and had little to no mixing with the regional groundwater (Walker *et al*, 2018).

Samples that plot on the meteoric water line indicate direct recharge where no prior evaporation took place. Close clustering of the samples would suggest that the recharge occurred from the same event (or same recharge source) and that the groundwater is connected. From the current study results, the groundwater samples do not appear to be clustered in one space and this suggests different recharge events and or sources.

The source of moisture can be traced by using d-excess values. The d-excess was calculated from the LMWL equation as presented in Figure 5-18. The results from the calculations are presented in Table 5-9, the d-excess values range from -0.98‰ to 10.19‰. This big range indicates the possible existence of different moisture sources for rainfall in the area. D-excess values from the boreholes are consistent with the observations from the $\delta\ ^{18}O$ and δD indicating different moisture sources, this is presented in different clusters i.e. A and B. Cluster A, the high d excess indicates the influence of local moisture source to the rainfall in the area that contributed to the water system. Cluster B is atmospheric moisture not influenced by secondary evaporative processes (d-excess =10 ‰) and also indicates local moisture source (Marfia *et al*., 2004). Cluster A and B could both be from local moisture sources but the obvious separate clustering of the samples also suggests different recharge events. The surface water samples presented the highest stable isotope and

lowest d-excess values (sometimes negative) indicating strong evaporation and contribution of regional moisture source with enriched ^{18}O resulting from the evaporative effect.

Table 5-9: Stable Isotope data for the study area.

Sample Identification	δD (‰)	STD Deviation (‰)	$\delta^{18}O$ (‰)	STD Deviation (‰)	d-excess
IAL 1*	-15.0	0.0	-3.70	0.00	5.75
IAL 2*	-18.1	0.3	-4.22	0.02	5.51
IAL 3*	-18.0	0.1	-4.19	0.00	5.50
IAL 4*	-13.0	0.1	-3.93	0.02	9.04
IAL 5*	-13.0	0.1	-3.94	0.02	9.08
IAL 6*	-9.3	0.0	-3.47	0.00	10.13
IAL 7*	-17.4	0.1	-4.24	0.04	6.33
IAL 8**	+35.9	0.1	+6.27	0.06	0.79
IAL 9**	+21.5	0.3	+3.40	0.04	2.44
IAL 10**	+17.7	0.2	+268	0.01	2.68
IAL 11**	+36.8	0.3	+6.64	0.04	-0.39
IAL 12**	+32.2	0.5	+5.73	0.06	0.17
IAL 13**	+26.1	0.0	+4.84	0.00	-0.98
IAL 14**	+17.7	0.2	+3.18	0.01	-0.07
IAL 15**	+6.9	0.0	+0.61	0.00	3.54

*Groundwater samples,

** Surface water samples

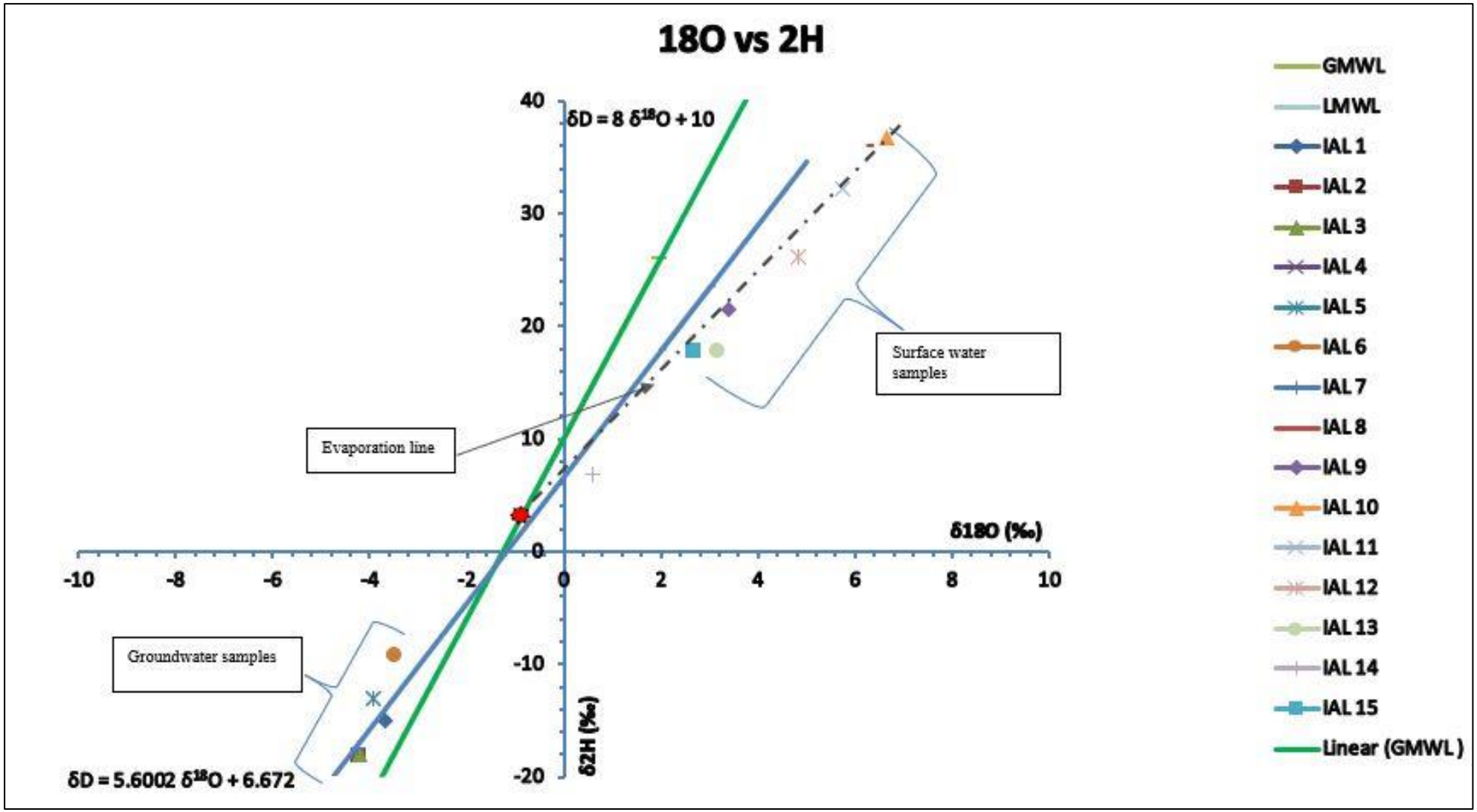

Figure 5-17: Plot of deuterium vs 18-Oxygen for the study area.

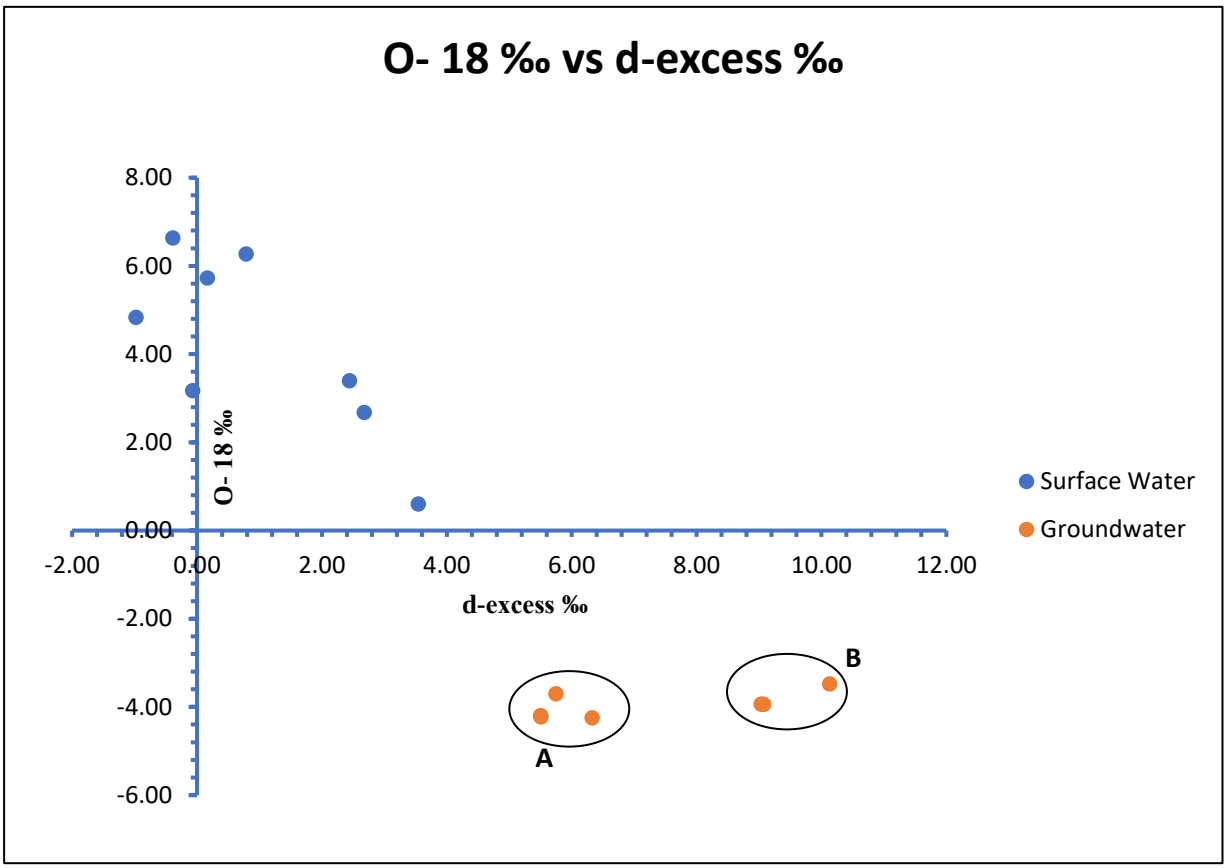

Figure 5-18: Deuterium excess vs 18-Oxygen for the study area. Clusters A and B represent different moisture source for the groundwater on site.

6.0 CONCEPTUAL HYDROGEOLOGICAL MODEL

A conceptual model of the study area is developed based on the fieldwork carried out as outlined in previous sections and the results from each task. The presented conceptual model summaries the results from the current hydrogeological study and is adopted as a reasonable representation of the hydrogeologic conditions of the area. It is important to note that during drilling, the mine voids were not intersected. The cross-section is drawn based on the line shown in Figure 3-2. The following points summaries the conceptual model (Figure 6-1) based on the results presented:

- The conceptual model shows a reconstruction of the site hydrostratigraphy based on the information obtained from the boreholes. The aquifer system within the study area can be divided into two different systems, the perched shallow aquifers which are hosted in the upper stratigraphy including sandstones and the deep aquifer which is hosted within the hard competent layers (dolerites) and are controlled by fractures.

- The ferricrete layers occur within the laterite zone and may hosts "pockets" of water which could also be classified as a perched aquifer. The layers occur in lenses within the laterite. This layer is visible on the Lottering quarry face and was intercepted in the boreholes at varying thicknesses. The average depth of these layers is 4 – 8 mbgl.

- The study area is underlain by alternating fine-grained sandstones and carbonaceous siltstone of the Vryhied Formation. These Karoo sediments were intruded by dolerite sills, creating interfingered, and mostly impermeable layers within the sedimentary sequence. The contacts between the sill and the host rock are likely to have an increased hydraulic conductivity, due to the fracturing that occurred during the intrusion, which provides preferential flow for groundwater. The sills themselves appear to be massive and water-tight, and would act as aquitards, creating perched aquifers where percolated water from recharge collects above the water table.

- The base of the quarries extends to about 15 mbgs, and mining was ceased at that depth due to the compaction of the material. There is a dolerite sill of considerable thickness (> 30 m) in the area of Quarry 1 to 3, at a depth of 20 mbgs, and this intrusion probably resulted in contact metamorphism of the Ecca sediments. This metamorphism would result in harder, less permeable rock. This also provides clues as to why the water on the surface is not locally connected to the regional aquifer.

- The isotopes data also showed no evidence of interconnectivity between surface and groundwater due to differences in isotopic signature. A combination of isotopes and hydrochemical analysis suggests that abandoned deep coal mining has no link or influence of current surface water and the shallow aquifers identified in the study area.

- Recharge to the deep aquifers locally is expected to be minimal due to the existence of sills and dykes in the area.

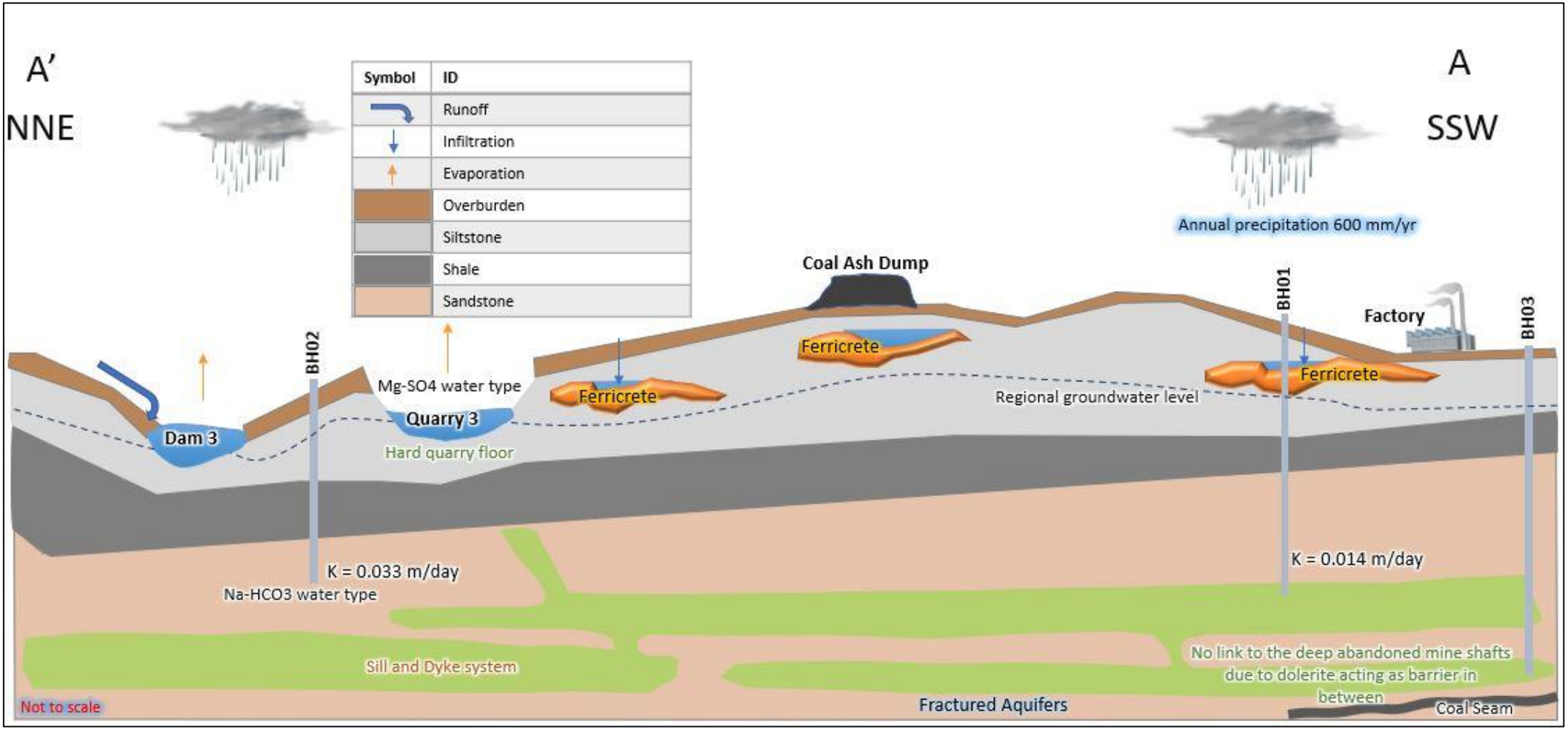

Figure 6-1. Conceptual hydrogeological Model for the study area.

7.0 CONCLUSIONS AND RECOMMENDATIONS

The hydrogeological conditions of the Corobrik Glencoe Factory are investigated in the present study. A combination of methods (i.e. Piper diagrams, Durov diagrams, Gibbs diagrams, ionic ratios, isotopic analyses etc) proved to be efficient in analysing the groundwater chemistry and origin/sources of the water. The acquired data using the different methods provided input data that is utilised in the development of a hydrogeological conceptual site model for the Glencoe factory.

The geology of the area is mainly represented by the Ecca Group rocks consisting of a metasedimentary sequence with dolerite dykes and sills interfingering with this sequence. Two aquifer systems are identified in this study and are hosted within the upper sequence comprising of sandstones and the dolerites at depth. The upper sequence of sandstones presents perched shallow aquifers, while the deep aquifer is made up of the hard competent layers (dolerites) and is controlled mainly by secondary permeabilities which are as a result of fracturing that occurred during the emplacement of the dolerite dykes and sills. Aquifer tests using slug test on the newly drilled boreholes on site estimated hydraulic conductivity of 0.014 - 0.033 m/day and transmissivity values ranging from 0.44 m^2/day to 1.19 m^2/day.

The mine footprint within the area is visible in the surface water and also assumed to occur underground within the property particularly related to old underground mine workings. The impact on groundwater from this footprint appears to be non-existent. Groundwater analysis showed that the dominant anion is bicarbonate, with pH values indicating that the water is neutral. This water is fresh and indicates that it is recently recharged through the soil horizon that is bicarbonate rich. The EC and TDS measurements parallel this observation, confirming fresh groundwater. The close clustering that was observed in the piper diagrams with the confirmation from the Durov Diagram suggested that calcium may be exchanged for sodium in some samples. Further analysis using the Durov diagram showed that the process of ion exchange may be already occurring as it was observed that samples plotted towards the sodium field from the calcium field, it was also noted that the sodium ion was the dominant cation. The occurrence of magnesium and calcium with sulphate was found to not be concomitant. This suggested that AMD was not a controlling factor to the groundwater chemistry, this observation was also supported by plot of total cations vs chloride + sulphate.

The impact on surface water from the mine footprint is somewhat existent, although it is negligible at the present moment. The dominant water type was found to be calcium bicarbonate. Which represents fresh water. Two other minor water types, magnesium sulphate and sodium bicarbonate where also identified for the surface water. Very few samples plotted in the AMD field and was suggestive of sulphate influencing the water chemistry. The sulphate source is the visible coal discard dumps on the surface.

A common piper plot reveals that the chemistry of the groundwater and surface water varies distinctly. The groundwater was more sodium bicarbonate concentrated while the surface water was calcium bicarbonate concentrated and was clustered towards the upper quadrant of the piper diagram. This indicates that the two systems are not hydraulically connected or at least one does not influence the other. This observation is further proved by the use of stable isotopes where it was observed that the groundwater and surface water samples plotted in different regions. D-excess values for surface water revealed a strong evaporation trend and suggested that the water had no influence or contribution to the groundwater.

Isotope data identified that the groundwater is from different recharge sources and or events. The surface water showed a strong evaporative signal, as it would be expected. No connectivity could be identified between the groundwater and surface water within the site using isotopic analysis.

In order to improve the knowledge and understanding of the site in terms of hydrogeological processes, more work needs to be done, from the results of the study conducted presently, it is recommended that:

1. Drill deeper boreholes to intersect the old shafts and get water samples and assess if there is any impact of the old mining shafts.

2. It is also recommended for the factory that the boreholes drilled be included in the monitoring program. It is noted that currently, only quarry water monitoring is in place.

3. It is recommended that soil samples be taken to do geochemical analysis on them and also do analysis of the ash dumps.

8.0 REFERENCES

Akcil, A. and Koldas, S. 2006 Acid Mine Drainage (AMD) Causes, Treatment and Case Studies. Journal of Cleaner Production, 14, 1139-1145.

Aly, A. A, Al-Omran, A.M and Alharby, M. M. 2014. The water quality index and hydrochemical characterization of groundwater resources in Hafar Albatin, Saudi Arabia. Arab J Geosci 8. 4177-4190.

Al-Aboodi, A, H, Al-Tai, M, A, and Al-Khadhimi, A, M. 2008. Hydrochemical Classification of Groundwater in Safwan - Al-Zubair Area, South of Iraq. Marsh Bulletin 3(1). 45-56.

Barnes, M, R and Vermeulen, P, D. 2012. Guide to groundwater monitoring for the coal industry Water SA Vol. 38 No. 5. 831 – 836.

Bear, J, Beljin, M, S and Ross, R, R. 1992. Fundamentals of Ground-Water Modeling. The United States Environmental Protection Agency. 540/S-92/005. 1- 11.

Campaner, V, P, Luiz-Silva, W and Machado, W. 2014. Geochemistry of acid mine drainage from a coal mining area and processes controlling metal attenuation in stream waters, southern Brazil. Annals of the Brazilian Academy of Sciences. 86(2): 539 – 554.

Catuneanu, O, Wopfner, H, Eriksson, P, Cairncross, B, Rubidge, B, Smith, R. and Hancox, P. 2005. The Karoo basins of south-central Africa, Journal of African Earth Sciences. 43. 211-253.

Clark I, D, and Fritz P. 1997. Environmental Isotopes in Hydrogeology. New York. Lewis Publishers. pp 352.

Corobrik (Pty) Ltd. 2011. Mandatory C.O.P. to Combat Rockfall and Slope Instability Related Accidents at Corobrik Glencoe Surface Mine. An internal Report. pp 50.

Corobrik (Pty) Ltd. 2017. Corobrik Glencoe Surface Mine Code of Practice. An internal Report. pp 32.

Cravotta, C, A. 2005. Effects of abandoned coal-mine drainage on streamflow and water quality in the Mahanoy Creek Basin, Schuylkill, Columbia, and Northumberland Counties,

Pennsylvania, 2001: U.S. Geological Survey Scientific Investigations Report 2004-5291, 60.

Department of Water Affairs and Forestry. 2004. Thukela Water Management Area Internal Strategic Perspective. pp 178.

Department of Water Affairs and Forestry. 2006. Best Practice Guideline G3. Water Monitoring Systems. pp 43.

Dlamini, A. E and Demlie, M. 2020. Integrated hydrogeological, hydrochemical and environmental isotope investigation of the area around the Kusile Power Station, Mpumalanga, South Africa. Journal of African Earth Sciences (172) pp 103958.

Freeze, R.A., and Cherry, J.A. 1979. Groundwater. New Jersey: Prentice Hall Inc. pp 604.

Ghesquière, O. Walter, J. Chesnaux, R and Rouleau, A. 2015. Scenarios of groundwater chemical evolution in a region of the Canadian Shield based on multivariate statistical analysis. Journal of Hydrology: Regional Studies. 4. 246–266.

Gomo, M and Vermeulen D. 2014. Hydrogeochemical characteristics of a flooded underground coal mine groundwater system. Journal of African Sciences. 92. 68-75.

Halim, M.A. Majumder, R.K. Zaman, M.N and Hossain S.M. 2012. Mobility and impact of trace metals in Barapukuria coal mining area, Northwest Bangladesh. Arabian Journal of Geosciences. 6, 4593–4605.

Hancox, P, J and Gotz, A, E. 2014. South Africa's coalfields – a 2014 perspective. International Journal of Coal Geology 132. 170–254.

Henning, D. 2016. uMzinyathi District Municipality Environmental Management Framework Status Quo Report. Prepared for uMzinyathi District Municipality by Nemai Consulting. Unpublished Report. pp 182.

Hiscock, K, M. 2005. Hydrogeology: principles and practice. Blackwell Science Ltd, Australia. pp 544.

Huang, X, Wang, G, Liang, X. Linfeng C, Luan M and Qingyu Xu, Q. 2018. Hydrochemical and Stable Isotope (δ D and δ^{18}O) Characteristics of Groundwater and Hydrogeochemical Processes in the Ningtiaota Coalfield, Northwest China. Mine Water Environ 37, 119–136.

Ismael, I.R. 2016. Slug Tests in Unconfined Aquifers. Unpublished Master's Thesis at Western Michigan University.

Johnson, M. R. van Vuuren, C.J. Visser, J. N. J. Cole, D. I. Wickens, D. de V., Christie, A. D. M., Roberts, D. L. Brandl, G. 2006. Sedimentary rocks of the Karoo Supergroup. In: Johnson, M.R., Anhaeusser, C. R and Thomas, R. J. (Eds.), The Geology of South Africa. Geological Society of South Africa, Johannesburg/Council for Geoscience, Pretoria, 461-499.

Kendall C, Caldwell E. A. 1998. Fundamentals of Isotope Geochemistry, in: Isotope Tracers in Catchment Hydrology, edited by Kendall C and McDonnell JJ. Elsevier Science, Amsterdam. 51 – 86.

Konikow, L. F and Reilly, T. E. 1999. Groundwater Modelling: The Handbook of Groundwater Engineering. US Geological Survey. Boca Raton: CRC Press. pp 1092.

Kshetrimayum, K.S and Laishram, P. 2020. Assessment of surface water and groundwater interaction using hydrogeology, hydrochemical and isotopic constituents in the Imphal river basin, Northeast India. Groundwater for Sustainable Development. 11.

Lapworth, D. J, Nkhuwa, D. C. W, Okotto-Okotto, J, Pedley, S, Stuart, M. E, Tijani, M. N and Wright, J. 2017. Urban groundwater quality in sub-Saharan Africa: current status and implications for water security and public health. Hydrogeol J. 25 (4). 1093-1116.

Lei, M, Qi-yan, F, Lai, Z, Ping, L, Qing-Jun, M. 2009. Environmental cumulative effects of coal underground mining. Procedia Earth and Planetary Science. (1)1280–1284.

Lghoul, M, Maqsoud, A, Hakkou, R, Kchikach, A. 2014. Hydrogeochemical behaviour around the abandoned Kettara mine site, Morocco. Journal of Geochemical Exploration 144. 456–467.

Li, J, Wang, W., Wang, D, Li, J. and Dong, J. 2020. Hydrochemical and Stable Isotope Characteristics of Lake Water and Groundwater in the Beiluhe Basin, Qinghai–Tibet Plateau. Water, 12(8), pp 2269.

Maidment, D. R. and Hooper, R. P. 2005. Conceptual Framework. In: D.R. Maidment, ed. Hydrologic information system status report, chap. 2. Washington, DC: Consortium of Universities for the Advancement of Hydrologic Science, Inc (CUAHSI), 7–23.

Marfia, A.M. Krishnamurthy, R.V. Atekwana, E.A. and Panton, W.F. 2004. Isotopic and geochemical evolution of ground and surface waters in a karst dominated geological setting: a case study from Belize, Central America. Applied Geochemistry. 19, 937-946.

Matoti, A, Conrad, J, and Susan, J. 1999. Aquifer Classification of South Africa Map, Department of Water Affairs.

Mazor E. 2004. Chemical and isotopic groundwater hydrology (Third Edition). Marcel Dekker, Inc., 270 Madison Avenue, New York, pp 438.

McCarthy, T, S and Humphries, M, S.2013. Contamination of the water supply to the town of Carolina, Mpumalanga, January 2012. S Afr J Sci.; 109(9/10). 1 – 10.

Mohanty, A.K, Lingaswamy, M, Gurunadha Rao, V. V. S, and Sankaran, S. 2018. Impact of acid mine drainage and hydrogeochemical studies in a part of Rajrappa coal mining area of Ramgarh District, Jharkhand State of India. Groundwater for Sustainable Development. (7) 164–175.

Mook, W. G. 2000. Environmental Isotopes in the hydrological cycle. Principles and applications. International Atomic Energy Agency and United Nations Educational, Scientific and Cultural Organization. Vol 1. 35-36.

Nadiri, A.A. Moghaddam, A.A. Tsai, F.T. and Fijani, E. 2013. Hydrogeochemical analysis for Tasuj plain aquifer, Iran. J Earth Syst Sci 122, 1091–1105.

Prathap, A and Chakraborty, S. 2019. Hydro chemical characterization and suitability analysis of groundwater for domestic and irrigation uses in open cast coal mining areas of Charhi and Kuju, Jharkhand, India. Groundwater for Sustainable Development. (9) p100244.

Salman, S.A, Melegy, A.A, Shaban, A.M. and Hassaan, M.M. 2013. Hydrogeochemical Characteristics and classification of Groundwater in Sohag Governorate, Egypt. Journal of Applied Sciences Research, 9(1): 758-769.

Singhal, B, B, S. Gupta, R,P. 2010. Applied Hydrogeology of Fractured Rocks(Second Edition). Springer, New York. 325-327.

Statistics South Africa., 2011. Census 2011. Web link: http://www.statssa.gov.za/?page_id=993&id=endumeni-municipality.

Tarawneh, M,S,M. Janardhana, M.R and Ahmed, M.M. 2019. Hydrochemical processes and groundwater quality assessment in North eastern region of Jordan valley, Jordan. HydroReserch. Volume 2. 129-145.

Umgeni. 2019. Infrastructure Master Plan 2019. Volume 6: Upper uThukela System.

Uys, J. 2007. Lithostratigraphy. Depositional environments and sedimentology of the Permian Vryhied formation (Karoo Supergroup). Arnot North, Witbank coalfield, South Africa. University of Johannesburg. Unpublished Master's Thesis. pp 132.

Walker, D. Jovanovic, N. Bugan, R. Abiye, T. du Preez, D. Parkina, G. and Gowing, J. 2018. Alluvial aquifer characterisation and resource assessment of theMolototsi sand river, Limpopo, South Africa. Journal of Hydrology: Regional Studies. 19, 177-192.

Waaterboards 2020. Alkalinity Conversions. Online Source:

https://www.waterboards.ca.gov/drinking_water/certlic/drinkingwater/documents/drinkingwaterlabs/AlkalinityConversions.pdf.

Wilson, A, S. 2005. Hydrogeology, conceptual model, and groundwater flow within alluvial aquifers of the Tenthill and Ma Ma catchments, Lockyer Valley, Queensland (Doctoral dissertation, Queensland University of Technology). pp 141.

Woodford, A and Chevallier, L. 2002. Hydrogeology of the Main Karoo Basin: current knowledge and future research needs, Water Research Commission Report TT179/02, Pretoria, South Africa. pp 482.

Yang, X, Steward, D. R, de Lange, W. J, Lauwo, S. Y , Chubb, R. M and Bernard, E. A. 2010. Data model for system conceptualization in groundwater studies, International Journal of Geographical Information Science, 24:5, 677-694.

9.0 APPENDICES

1. Borehole logs for the study area

BOREHOLE ID					
BH01	PROJECT NAME	MSc Research Project	LATITUDE	-28.14615
	PROJECT NO		LONGITUDE	30.13316
	CLIENT NAME:	Corobik	ELEVATION	1355.01
	LOCATION	Kwazulu Natal	EOH DEPTH	50
	DATE DRILLED	14/9/2018	FARM NAME	BRICKFIELD
	COORD. SYST	WGS 84	DIP	90
			AZIMUTH	0

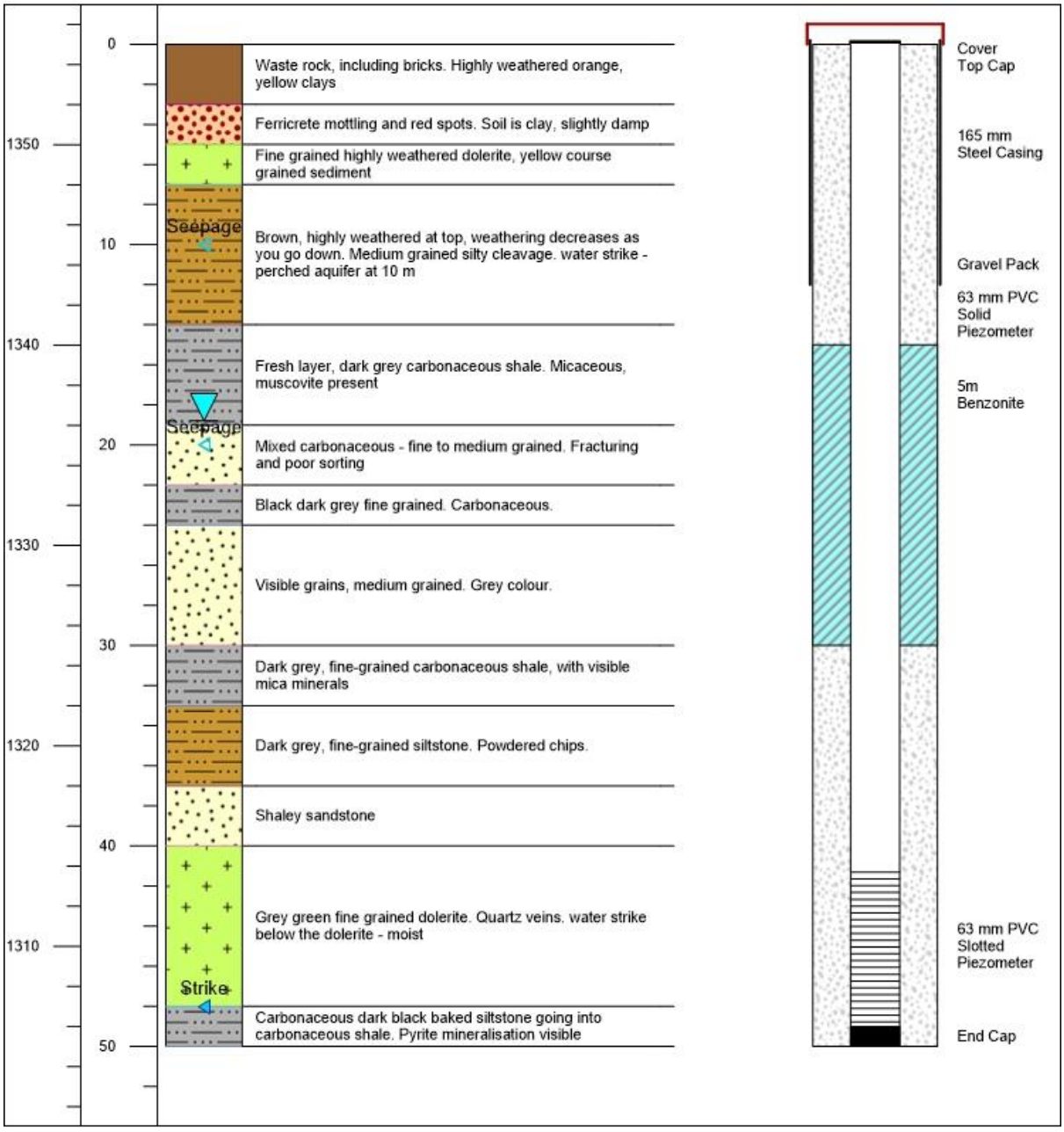

NOTES	
	Water strike at 48m Yield: 1.67 m³/sec pH: 8.9 TDS: 120.00 mg/L EC: 0.25 mS Temp: 19.2°C

BOREHOLE ID **BH01**

WITS UNIVERSITY

BOREHOLE ID					
BH02	PROJECT NAME	MSc Research Project	LATITUDE	-28.14884
	PROJECT NO		LONGITUDE	30.14796
	CLIENT NAME:	Corobik	ELEVATION	1352.02
	LOCATION	Kwazulu Natal	EOH DEPTH	50
	DATE DRILLED	16/9/2018	FARM NAME	BRICKFIELD
	COORD. SYST	WGS 84	DIP	90
			AZIMUTH	0

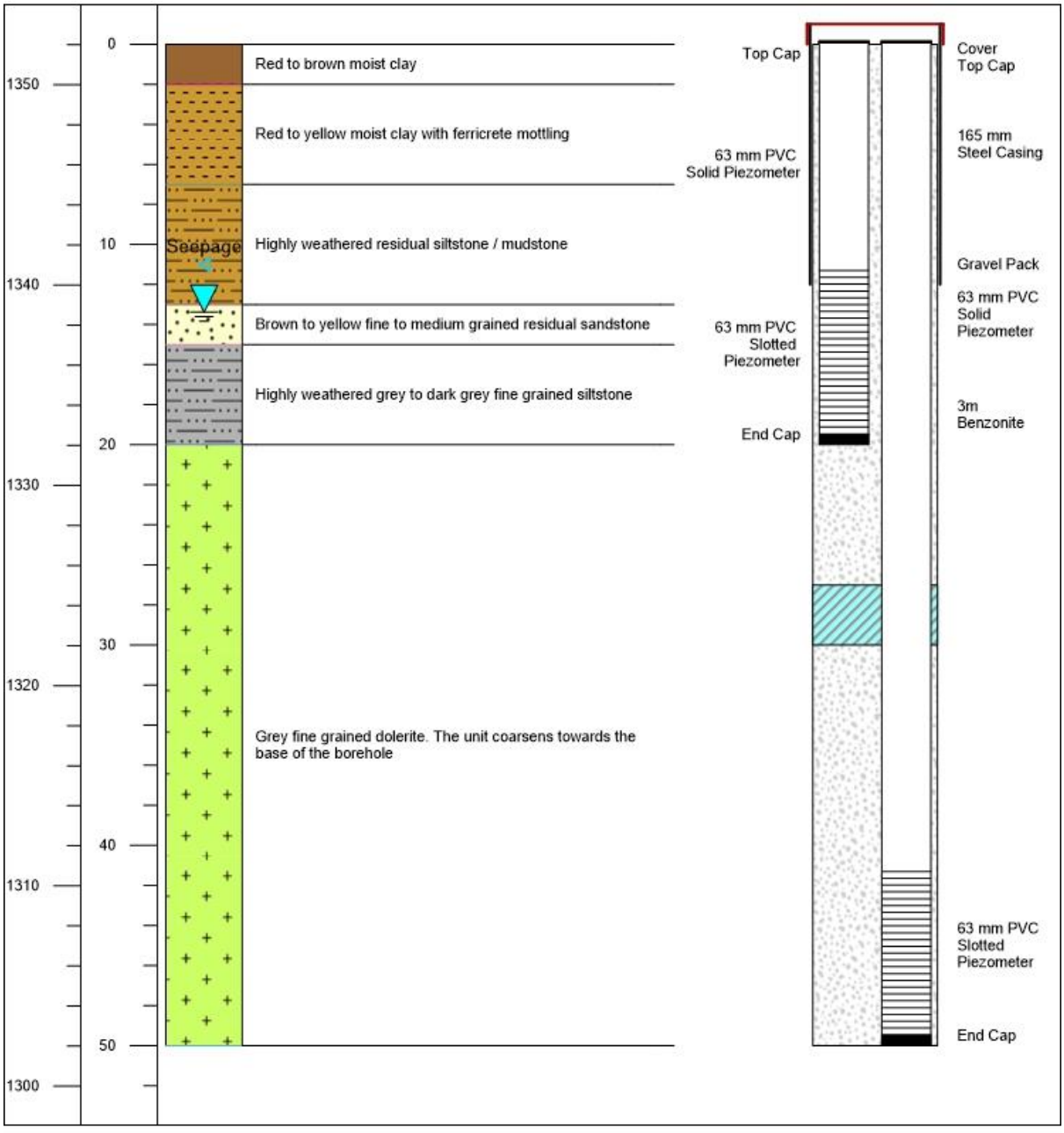

NOTES

Water strike at 48m
Yield: 1.67 m³/sec
pH: 8.9
TDS: 120.00 mg/L
EC: 0.25 mS
Temp: 19.2°C

BOREHOLE ID **BH02**

WITS UNIVERSITY

BOREHOLE ID					
BH03	PROJECT NAME	MSc Research Project	LATITUDE	-28.1542
	PROJECT NO		LONGITUDE	30.13294
	CLIENT NAME:	Corobik	ELEVATION	1360
	LOCATION	Kwazulu Natal	EOH DEPTH	50
	DATE DRILLED	19/9/2018	FARM NAME	BRICKFIELD
	COORD. SYST	WGS 84	DIP	90
			AZIMUTH	0

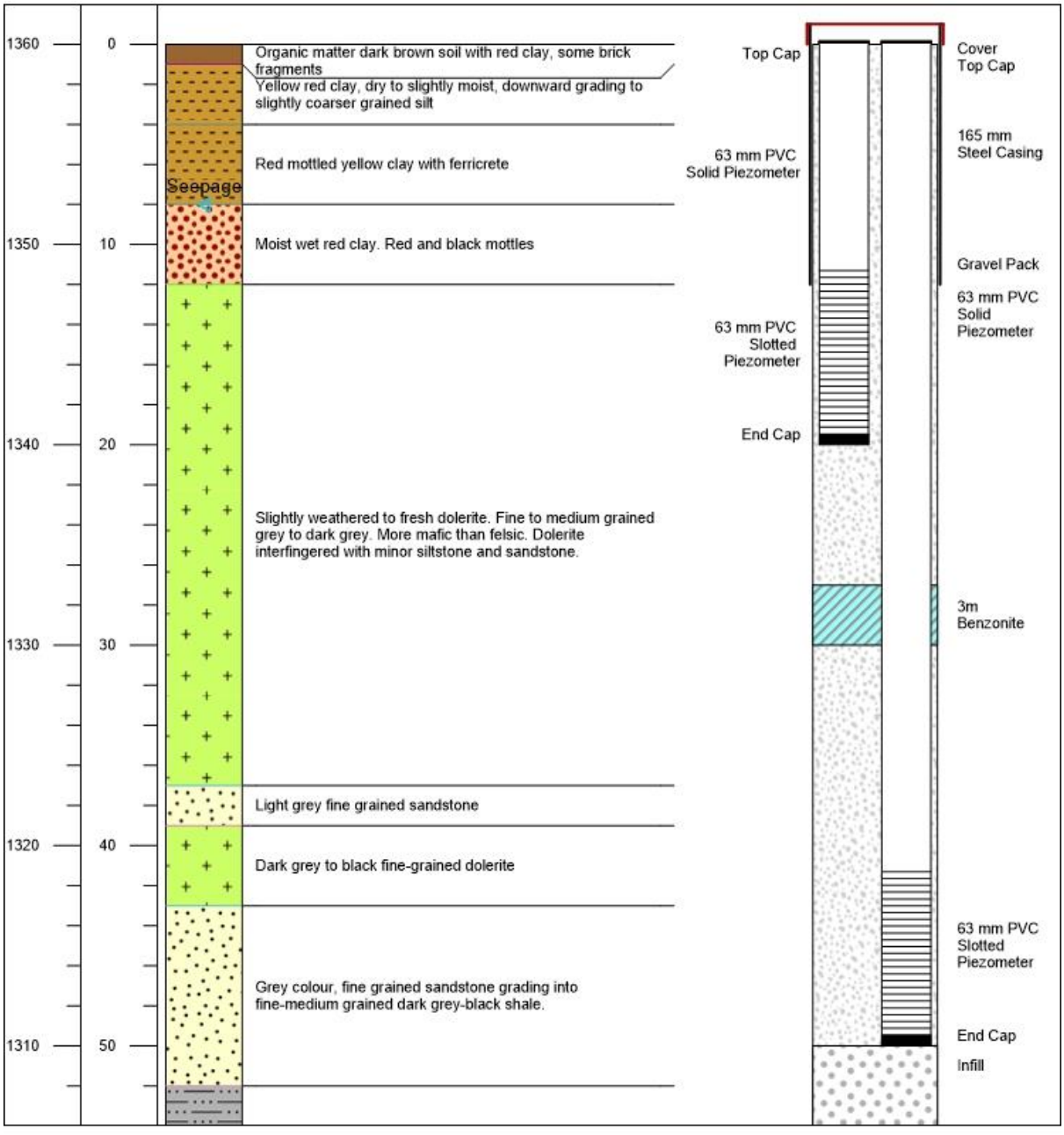

NOTES	Water strike at 48m Yield: 1.67 m³/sec pH: 8.9 TDS: 120.00 mg/L EC: 0.25 mS Temp: 19.2°C
PAGE 1 of 3	BOREHOLE ID **BH03**

WITS
UNIVERSITY

BOREHOLE ID	PROJECT NAME	LATITUDE
BH03	PROJECT NO	LONGITUDE
	CLIENT NAME:	ELEVATION
	LOCATION	EOH DEPTH
	DATE DRILLED	FARM NAME
	COORD. SYST	DIP
		AZIMUTH

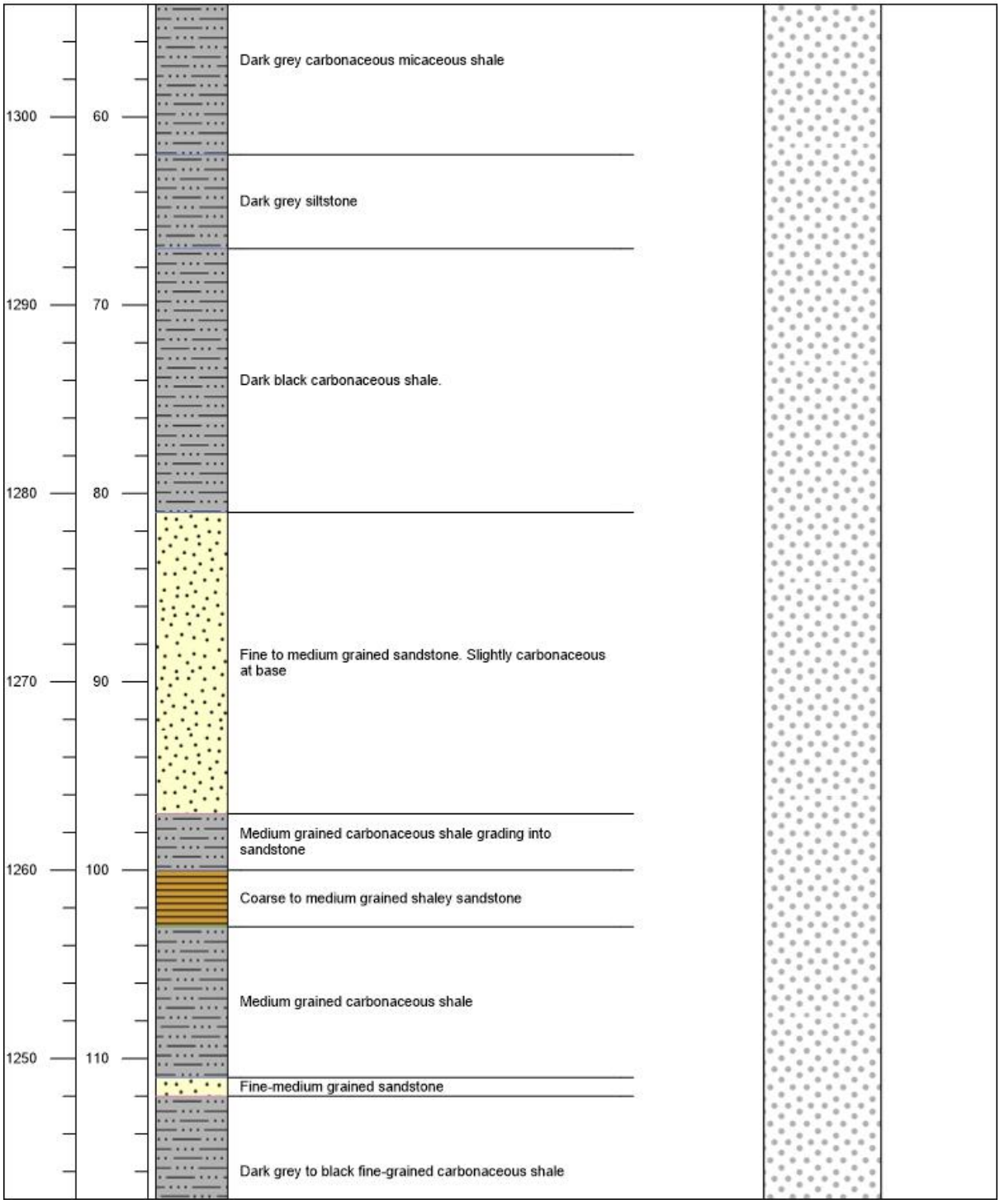

BOREHOLE ID	PROJECT NAME	LATITUDE
BH03	PROJECT NO	LONGITUDE
	CLIENT NAME:	ELEVATION
	LOCATION	EOH DEPTH
	DATE DRILLED	FARM NAME
	COORD. SYST	DIP
		AZIMUTH

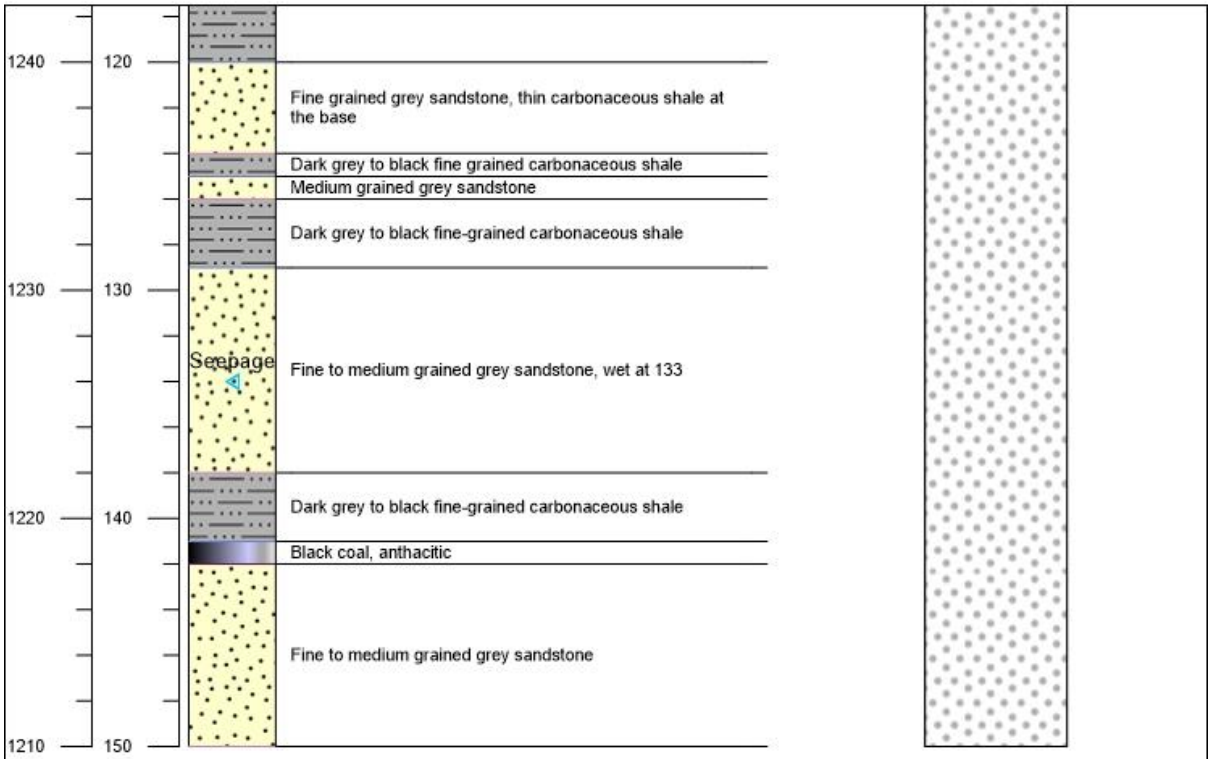

2. Spreadsheet for borehole logging

Boreholeid	Depth from	Depth to	Lithology	Lithology description
BH01	0	3	Overburden	Waste rock, including bricks. Highly weathered orange, yellow clays
BH01	3	5	Ferricete	ferricrete mottling and red spots. Soil is clay
BH01	5	7	Dolerite	fine grained and dry
BH01	7	14	Siltstone	brown, highly weathered at top, weathering decreases as you go down. Medium grained silty cleavage.
BH01	14	19	Shale	fresh layer, dark grey carbonaceous shale. Micaceous, mineral muscovite present
BH01	19	22	Sandstone	mixed carbonaceous - medium grained. Fracturing and poor sorting
BH01	22	24	Shale	black dark grey fine grained. Carbonaceous.
BH01	24	30	Sandstone	visible grains, medium grained. Grey color.
BH01	30	33	Shale	fine grained shale. Dark grey color. Visible mica. Carbonaceous.
BH01	33	37	Siltstone	dark grey fine grained. Powdered chips.
BH01	37	40	Shale	SHALY SANDSTONE
BH01	40	48	Dolerite	grey green fine grained dolerite. Qautz viens.
BH01	48	50	Shale	carbonaceous dark black color. Baked siltstone going into coal. Pyrite mineralisation visible
BH02	0	2	Overburden	red-brown clay- mosit
BH02	2	7	Clay	red- yelow clay, moist mottled
BH02	7	13	Siltstone	residual siltstone / mudstone. Highly weathered
BH02	13	15	Sandstone	brown - yellow fine to medium grained sandstone residual
BH02	15	20	Siltstone	highly weathered grey to dark grey. Fine graibned
BH02	20	50	Dolerite	grey -fine grained dolerite. The unit coarsens as you go down. See quartz mineralisation.
BH03	0	1	Overburden	organic matter dark brown soil with red clay
BH03	1	4	Clay	yellow red clay, dry to slightly moist, downward grading to slightly coarser grained silt
BH03	4	8	Ferricrete	red mottled yellow clay with ferricrete
BH03	8	12	Clay	moist wet red clay. Red and black mottles
BH03	12	37	Dolerite	slightly weathered to fresh dolerite. Fine to medium grained grey to dark grey. More mafic than felsic. Dolerote fingered. Occurs with minor siltstone and sandstone.
BH03	37	39	Sandstone	light grey fine grained sandstone
BH03	39	43	Dolerite	dark grey to black fine grained dolerite
BH03	43	52	Sandstone	grey color, fine grained sandstone grading into fine-medium grained dark grey-black shale.
BH03	52	62	Shale	dark grey micaceous shale. Carbonaceous.
BH03	62	67	Siltstone	dark - grey in color
BH03	67	81	Shale	dark black carbonaceous shale.
BH03	81	97	Sandstone	fine-medium grained sandstone. Slightly carbonaceous at base
BH03	97	100	Shale	medium grained carbonaceous shale. Shale grading into sandstone
BH03	100	103	Shaley-Sandstone	coarse medium grained.
BH03	103	111	Shale	medium grained carbonaceous shale.
BH03	111	112	Sandstone	fine-medium grained sandstone.
BH03	112	120	Shale	dark grey to black fine grained carbonaceous shale.
BH03	120	124	Sandstone	fine grained grey sandstone, carbonaceous thin shale at the base
BH03	124	125	Shale	carbonaceous shale. Dark grey to black fine grained shale.
BH03	125	126	Sandstone	medium grained grey sandstone
BH03	126	129	Shale	dark grey to black fine grained carbonaceous shale.
BH03	129	138	Sandstone	grey color. Fine grained.
BH03	138	141	Shale	dark grey to black fine grained carbonaceous shale.
BH03	141	142	Coal	
BH03	142	150	Sandstone	fine to medium grained grey sandstone

3. List of collected samples

Lab ID	Sample ID	Description	Type	pH	EC (mS)	TDS (ppt)	TDS (mg/l)	Temperature (°C)	X	Y	water level (mbgl)
IAL 1	GC01	BH01	Groundwater	7.93	0.43	0.41	410	18.8	218440.7	6883283.5	18.79
IAL 2	GC02S	BH02 Shallow	Groundwater	7.37	0.15	0.08	80	20.2	219902.03	6883019.5	13.38
IAL 3	GC02D	BH02 Deep	Groundwater	7.56	0.2	0.1	100	20.3	219902.03	6883019.5	15.22
IAL 4	GC03 (filtered)	BH04 - Shallow BH near BH01	Groundwater	8.27	0.38	0.19	190	21.9	218434.67	6883252	8.19
IAL 5	GC03 (unfiltered	BH04 - Shallow BH near BH01	Groundwater	8.27	0.38	0.19	190	21.9	218434.67	6883252	8.19
IAL 6	BH020	Monitoring BH near Dump and Roa	Groundwater	8.82	0.44	0.22	220	19.8	219028.96	6882964.7	4.74
IAL 7	GC07	Borehole on North farm	Groundwater	7.98	0.16	0.08	80	19.6	219976.34	6883978.2	18.6
IAL 8	DAM 1	Dam 1 (GCO6)	Surface Water	7.6	0.08	0.04	40	10.9	219999.44	6883099.4	
IAL 9	DAM 2	Dam 2	Surface Water	7.26	0.09	0.04	40	12.3	220001.2	6883267.2	
IAL 10	DAM 3	Dam 3 on north farm	Surface Water	7.39	0.09	0.04	40	19.1	219828.65	6883460.5	
IAL 11	O27 Quarry	Quarry 3	Surface Water	8.04	0.84	0.41	410	16	219145.49	6882850.6	
IAL 12	O28 Quarry	Quarry 1 (big one)	Surface Water	8.58	0.33	0.16	160	18.8	219673.21	6882955.1	
IAL 13	O21 Quarry	Shale Quarry North	Surface Water	8.7	1.84	0.92	920	18.2	218498.28	6883018.8	
IAL 14	O22 Quarry	Shale Quarry South	Surface Water	8.01	1.82	0.91	910	18.9	218468.73	6882979.3	
IAL 15	Prison Dam	Prison Dam	Surface Water	7.26	0.29	0.14	140	16	218261.19	6881781.7	

4. Slug test data

Borehole ID	Elapsed time (min)	Elapsed Time (sec)	Depth to water (mbgl)	h	h/h0	Time (seconds)	Time (Seconds) Zerod	Displacements (m)
BH1	1.55	115	18.65	0.10	1.000	93.00		0.10
BH1	3.02	182	18.68	0.07	0.700	181.20		0.07
BH1	3.36	216	18.69	0.06	0.600	201.60		0.06
BH1	3.59	239	18.70	0.05	0.540	215.40		0.05
BH1	4.31	271	18.70	0.05	0.500	258.60		0.05
BH1	5.02	600	18.72	0.04	0.350	301.20		0.04
BH1	5.30	303	18.71	0.04	0.400	318.00		0.04
BH1	5.48	348	18.71	0.04	0.400	328.80		0.04
BH1	6.29	389	18.72	0.04	0.350	377.40		0.04
BH1	7.00	420	18.72	0.03	0.300	420.00		0.03
BH1	7.30	450	18.72	0.03	0.300	438.00		0.03
BH1	8.04	484	18.72	0.03	0.300	482.40		0.03
BH1	8.35	515	18.73	0.02	0.250	501.00		0.02
BH1	9.01	541	18.73	0.02	0.200	540.60		0.02
BH1	9.31	571	18.73	0.02	0.200	558.60		0.02
BH1	10.01	601	18.73	0.02	0.200	600.60		0.02
BH1	10.47	647	18.73	0.02	0.200	628.20		0.02
BH1	11.45	705	18.74	0.02	0.150	687.00		0.02
BH1	12.48	768	18.74	0.01	0.140	748.80		0.01
BH1	13.48	828	18.74	0.01	0.140	808.80		0.01
BH1	15.00	900	18.74	0.01	0.110	900.00		0.01
BH1	16.32	992	18.74	0.01	0.110	979.20		0.01
BH1	18.00	1080	18.74	0.01	0.100	1080.00		0.01
BH1	20.05	1205	18.74	0.01	0.100	1203.00		0.01
BH1	21.58	1318	18.74	0.01	0.100	1294.80		0.01
BH1	27.00	1620	18.74	0.01	0.090	1620.00		0.01
BH1	37.09	2229	18.74	0.01	0.070	2225.40		0.01

Borehole ID	Elapsed time (min)	Elapsed Time (sec)	Depth to water (mbgl)	h	h/h0	Time (seconds)	Time (Seconds) Zerod	Displacements (m)
BH2	0.32	32.00	13.32	0.07	1.00	19.20		0.07
BH2	1.01	61.00	13.33	0.06	0.86	60.60		0.06
BH2	1.37	97.00	13.34	0.05	0.79	82.20		0.05
BH2	2.02	122.00	13.34	0.05	0.71	121.20		0.05
BH2	2.32	152.00	13.35	0.04	0.64	139.20		0.04
BH2	3.02	182.00	13.35	0.04	0.57	181.20		0.04
BH2	3.30	210.00	13.36	0.04	0.50	198.00		0.04
BH2	4.01	241.00	13.36	0.03	0.49	240.60		0.03
BH2	4.31	271.00	13.36	0.03	0.43	258.60		0.03
BH2	5.00	305.00	13.36	0.03	0.40	300.00		0.03
BH2	5.33	333.00	13.36	0.03	0.37	319.80		0.03
BH2	6.02	362.00	13.37	0.03	0.36	361.20		0.03
BH2	6.35	395.00	13.37	0.02	0.34	381.00		0.02
BH2	6.58	418.00	13.37	0.02	0.33	394.80		0.02
BH2	7.31	451.00	13.37	0.02	0.29	438.60		0.02
BH2	7.56	476.00	13.37	0.02	0.27	453.60		0.02
BH2	8.48	528.00	13.37	0.02	0.26	508.80		0.02
BH2	9.32	572.00	13.37	0.02	0.24	559.20		0.02
BH2	10.30	630.00	13.37	0.02	0.23	618.00		0.02
BH2	11.29	689.00	13.38	0.02	0.21	677.40		0.02
BH2	12.37	757.00	13.38	0.02	0.21	742.20		0.02
BH2	13.29	809.00	13.38	0.01	0.20	797.40		0.01
BH2	14.31	871.00	13.38	0.01	0.20	858.60		0.01
BH2	16.30	990.00	13.38	0.01	0.19	978.00		0.01
BH2	18.27	1107.00	13.38	0.01	0.19	1096.20		0.01
BH2	20.28	1228.00	13.38	0.01	0.17	1216.80		0.01
BH2	23.01	1381.00	13.38	0.01	0.17	1380.60		0.01
BH2	25.05	1505.00	13.38	0.01	0.16	1503.00		0.01
BH2	26.56	1616.00	13.38	0.01	0.14	1593.60		0.01
BH2	30.02	1802.00	13.38	0.01	0.14	1801.20		0.01
BH2	35.00	2135.00	13.38	0.01	0.14	2100.00		0.01
BH2	39.57	2397.00	13.38	0.01	0.14	2374.20		0.01
BH2	49.59	2999.00	13.38	0.01	0.14	2975.40		0.01

5. Groundwater chemistry results

Sample Mark	IAL 1	IAL 2	IAL 3	IAL 4	IAL 5	IAL 7	IAL 10	IAL 15
Silver as Ag mg/l	<0.004	<0.004	<0.004	<0.004	<0.004	<0.004	<0.004	<0.004
Aluminium as Al mg/l	4.46	40	22	0.18	0.14	0.14	4.28	0.90
Arsenic as As mg/l	<0.001	<0.001	<0.001	<0.001	<0.001	<0.001	<0.001	<0.001
Boron as B mg/l	<0.006	<0.006	<0.006	0.012	0.064	<0.006	<0.006	0.012
Barium as Ba mg/l	0.43	0.62	0.48	0.011	0.011	0.001	0.047	0.14
Beryllium as Be mg/l	<0.002	0.002	<0.002	<0.002	<0.002	<0.002	<0.002	<0.002
Bismuth as Bi mg/l	<0.005	<0.005	<0.005	<0.005	<0.005	<0.005	<0.005	<0.005
Cadmium as Cd mg/l	<0.001	<0.001	<0.001	<0.001	<0.001	<0.001	<0.001	<0.001
Cobalt as Co mg/l	0.005	0.061	0.013	<0.001	0.001	0.002	0.002	0.002
Chromium as Cr mg/l	0.039	0.25	0.054	<0.003	<0.003	<0.003	0.010	<0.003
Copper as Cu mg/l	0.056	0.18	0.042	0.004	0.014	0.029	0.011	0.002
Iron as Fe mg/l	10.10	84	26	0.34	5.35	6.93	5.77	1.18
Manganese as Mn mg/l	0.31	1.75	0.42	0.015	0.055	0.099	0.071	0.16
Molybdenum as Mo mg/l	<0.001	<0.001	<0.001	<0.001	<0.001	<0.001	<0.001	<0.001
Nickel as Ni mg/l	0.015	0.10	0.037	<0.003	0.003	<0.003	0.003	<0.003
Lead as Pb mg/l	0.037	0.076	0.023	0.005	0.003	0.005	0.009	<0.001
Phosphorus as P mg/l	0.20	1.13	0.44	<0.04	0.087	0.12	<0.04	0.095
Antimony as Sb mg/l	<0.01	<0.01	<0.01	<0.01	<0.01	<0.01	<0.01	<0.01
Selenium as Se mg/l	<0.001	<0.001	<0.001	<0.001	<0.001	<0.001	0.013	<0.001
Tin as Sn mg/l	<0.02	<0.02	<0.02	<0.02	<0.02	<0.02	<0.02	<0.02
Strontium as Sr mg/l	1.18	0.12	0.12	0.44	0.45	0.098	0.020	0.16
Titanium as Ti mg/l	0.085	0.35	0.025	<0.001	<0.001	<0.001	0.020	0.002
Thallium as Tl mg/l	<0.009	<0.009	<0.009	<0.009	<0.009	<0.009	<0.009	<0.009
Uranium as U mg/l	<0.004	<0.004	<0.004	<0.004	<0.004	<0.004	<0.004	<0.004
Vanadium as V mg/l	0.015	0.16	0.049	<0.002	<0.002	<0.002	0.025	0.004
pH Value @ 25°C	7.73	7.85	7.93	7.35	7.66	7.98	7.90	7.425
Conductivity @ 25°C mS/m	45.9	21.59	22.95	38.1	36.3	17.05	9.13	30.45
Total dissolved solids, TDS mg/l	270	136	142	162	184	88	111	160
Calcium as Ca mg/l	37.0	14.4	14.3	11.3	11.4	17.1	3.1	18.4
Calcium Hardness as $CaCO_3$ mg/l	92	36	36	28	28	43	8	46
Magnesium as Mg mg/l	9.66	4.80	6.52	10.31	10.26	4.93	2.53	8.30
Magnesium Hardness as $CaCO_3$ mg/l	40	19.75	27	42	42	20	10.40	34
Sodium as Na mg/l	42	21	24	43	42	11.68	9.78	26
Potassium as K mg/l	4.32	4.26	3.94	9.27	10.73	1.55	3.86	6.23
Total Alkalinity as CaCO3 mg/l	156	81	104	123	98	90	36	76
Chloride as Cl mg/l	11.50	2.94	2.67	8.67	9.95	<0.1	4.58	14.47
Sulphate as SO4 mg/l	81	21	11.00	32	34	2.57	9.42	43
Ammonium as NH4 mg/l	0.65	<0.1	<0.1	3.79	<0.1	<0.1	<0.1	<0.1
Ammonium as N mg/l	0.50	<0.10	<0.10	2.94	<0.10	<0.10	<0.10	<0.10
Nitrate as NO3 mg/l	0.3	5.1	2.1	16.8	31.2	0.5	1.5	7.2
Nitrate as N mg/l	<0.100	1.2	0.5	3.8	7.1	0.1	0.3	1.6
Fluoride as F mg/l	0.3	0.3	0.3	<0.1	<0.1	0.5	0.2	0.3
Zinc as Zn mg/l	0.027	0.21	0.041	<0.005	<0.005	<0.005	0.008	<0.005
Zirconium as Zr mg/l	0.005	0.021	0.012	<0.001	<0.001	<0.001	0.002	<0.001
Thorium as Th mg/l	<0.002	0.017	<0.002	<0.002	<0.002	<0.002	<0.002	<0.002
Mercury as Hg mg/l	<0.001	<0.001	<0.001	<0.001	<0.001	<0.001	<0.001	<0.001

6. Surface water chemistry results

Determinant	Maximum Allowable Limit (As per MHSA)	Dam (Gle/D/A)					Runoff Water from Workshop into Dams (Gle/D/B)			Quarry Next to Dam (Gle/Q/A)					Quarry North West of Factory (Gle/Q/B)				
		19/10/2016	23/01/2017	20/04/2017	25/05/2018	28/08/2018	19/10/2016	23/01/2017	25/05/2018	19/10/2016	23/01/2017	20/04/2017	25/05/2018	28/08/2018	19/10/2016	23/01/2017	20/04/2017	25/05/2018	28/08/2018
pH	ALL: 5.5 – 9.5 REC: 6 – 9	8.44	8.04	8.03	7.9	7.82	7.28	6.86	7.8	8.33	8.03	7.41	7.58	8.15	8.75	7.3	7.61	7.41	8.27
Conductivity (mS/m)	MAX: 300 REC: 70	79.7	75.6	74.8	77.2	181	68.6	49.8	20.4	64.7	75.7	14.9	182	15.3	198	110	119	181	79.9
Turbidity (NTU)	MAX: 5 REC: 1	14.3	2.73	2.86	3.85	0.934	11.6	6.34	0.56	27.5	2.42	5.42	2.42	3.03	2.31	0.62	2.14	2.84	5.21
Total Dissolved Solids (mg/l)	1000	588	576	522	532	1367	526	376	132	422	582	92	1572	93	1748	892	956	1552	508
Total Hardness (mg/l)	650	330	295	287	276	869	302	251	68	241	289	59	889	65	1069	492	597	852	308
Ammonia (mg/l)	1	BDL	BDL	BDL	BDL	<0.005	BDL	BDL	0.31	0.68	BDL	BDL	BDL	<0.005	0.21	BDL	BDL	BDL	<0.005
Magnesium (mg/l)	100	48.2	43	40.5	39.5	71.7	13.8	9.41	7.2	43.1	43.1	7.66	69.7	6.99	91.6	39.4	47.4	66.8	45.5
Calcium (mg/l)	150	52.9	47.4	48	45.6	230	97.9	77.4	15.3	25.6	44.5	11	241	14.6	277	132	161	231	48.4
Potassium (mg/l)	50	12	10.8	10.7	11.1	3.36	6.35	4.31	3.89	3.68	10	1.8	4.27	2.17	4.5	4.28	4.15	4.09	11.1
Sodium (mg/l)	400	60.5	52.9	47.9	50	97.2	35.1	16.5	13.2	67.3	45	12.1	101	8.95	117	48.5	62.3	97.3	49.4
Chloride (mg/l)	600	25	25	22.4	22	16.7	24.3	11.5	12.7	37.7	24.3	4.01	18.8	1.6	25.1	14.1	14.5	18.8	19.9
Sulphate (mg/l)	600	282	285	252	256	917	259	212	15.2	12.3	293	3.85	948	7.46	1099	552	583	950	246
Nitrite (mg/l)	Sum = 10	BDL	BDL	BDL	BDL	0.046	0.1	BDL	BDL	BDL	BDL	BDL	BDL	0.046	BDL	BDL	BDL	BDL	0.05
Nitrate (mg/l)		BDL	BDL	BDL	BDL	<0.194	0.52	0.35	BDL	BDL	0.1	BDL	BDL	<0.194	0.1	0.11	BDL	BDL	<0.194
Fluoride (mg/l)	1.5	0.69	0.64	0.59	0.55	0.45	0.98	0.55	0.2	0.96	0.68	BDL	0.28	0.468	0.32	0.31	0.41	0.28	0.845
Zinc (mg/l)	5	0.02	BDL	BDL	BDL	0.01	0.04	BDL	0.03	0.02	BDL	BDL	BDL	<0.002	0.02	BDL	0.01	BDL	0.004
Cadmium (µg/l)	20	BDL	BDL	BDL	BDL	<0.002	BDL	BDL	BDL	BDL	BDL	BDL	BDL	<0.002	BDL	BDL	BDL	BDL	<0.002
Copper (µg/l)	1000	BDL	BDL	1.53	BDL	<0.004	BDL	BDL	5.44	BDL	BDL	1.51	BDL	<0.002	BDL	BDL	1.61	BDL	**<0.002**
Iron (µg/l)	1000	71.9	19.7	BDL	BDL	<0.004	25.9	BDL	BDL	107	BDL	BDL	BDL	<0.004	65.6	200	BDL	BDL	**<0.004**
Lead (µg/l)	100	BDL	BDL	BDL	BDL	<0.004	BDL	BDL	BDL	BDL	BDL	BDL	BDL	<0.004	BDL	BDL	BDL	BDL	<0.004
Manganese (µg/l)	1000	BDL	14.3	BDL	BDL	<0.001	BDL	10.9	BDL	84.2	BDL	BDL	BDL	<0.001	BDL	BDL	BDL	BDL	<0.001
Selenium (µg/l)	50	3.15	1.1	6.11	BDL	<0.002	1.27	1.72	BDL	BDL	2.12	4.5	BDL	<0.002	2.9	BDL	5.65	BDL	<0.002